1 The *Drosophila* Cortactin Binding Protein 2 homolog, Nausicaa, regulates lamellipodial actin

2 dynamics in a Cortactin-dependent manner.

3

4 **Meghan E. O'Connell[1,2], Divya Sridharan[1,3], Tristan Driscoll[4], Ipsita Krishnamurthy[1], Wick**

5 **G. Perry[1], and Derek A. Applewhite[1]**

6 [1]Department of Biology, Reed College, Portland OR 97202 USA

7 [2]Department of Molecular Genetics and Cell Biology, University of Chicago, Chicago, IL 60637 USA

8 [3]Department of Biology, Boston College, Chestnut Hill, MA 02467

9 [4]Department of Cardiovascular Medicine, Yale University, New Haven CT 06511 USA

10

11 **Running Title:** Nausicaa alters actin dynamics

12

13 **Keywords:** Actin filament dynamics, cell migration

14
15

16 **Abstract.**

17 *Drosophila* CG10915 is an uncharacterized protein coding gene with sequence similarity to

18 human Cortactin Binding Protein 2 (CTTNBP2) and Cortactin Binding Protein 2 N-terminal like

19 (CTTNBP2NL). We have named this gene *Nausicaa* (*naus*) and characterize it through a

20 combination of quantitative live-cell total internal reflection fluorescence (TIRF) microscopy,

21 electron microscopy, RNAi depletion, and genetics. We found that Naus co-localizes with F-

22 actin and Cortactin in the lamellipodia of *Drosophila* S2R+ and D25c2 cells and this localization

23 is lost following Cortactin or Arp2/3 depletion or by mutations that disrupt a conserved proline

24 patch found in its mammalian homologs. Using Permeabilization Activated Reduction in

25 Fluorescence (PARF) and Fluorescence Recovery after Photo-bleaching (FRAP), we find that

26 depletion of Cortactin alters Naus dynamics leading to a decrease in its half-life. Furthermore,

27 we discovered that Naus depletion in S2R+ cells led to a decrease in actin retrograde flow and

28 a lamellipodia characterized by long, unbranched filaments. We demonstrate that these

29 alterations to the dynamics and underlying actin architecture also affect D25c2 cell migration

30 and decrease arborization in *Drosophila* neurons. We present the novel hypothesis that Naus

31 functions to slow Cortactin's disassociation from Arp2/3 nucleated branch junctions, thereby

32 increasing both branch nucleation and junction stability.

33

34

35

Introduction.

Cell migration is critical to a number of physiological processes including wound healing and immune function, development, neurogenesis, and vascularization. Aberrant cell migration is also the cause of a number of diseases including schizophrenia and mental disabilities, immunodeficiency, craniofacial disorders, and metastasis (Ridley et al., 2003). Cell migration relies heavily on the actin cytoskeleton, and the regulation of actin dynamics has major consequences for the underlying actin architecture dictating how cells migrate. Migration proceeds in four major steps - protrusion, adhesion, contraction, and retraction (Ridley et al., 2003). During the protrusion step of cell migration, the cell generates two major types of actin-based structures: lamellipodia and filopodia. While filopodia are characterized by parallel, unbranched actin filaments (Svitkina et al., 2003), the lamellipodia is composed of a densely branched network of actin filaments forming a sheet-like exploratory organelle (Abercrombie, M. et al., 1970). One protein that defines the lamellipodia is the actin-related protein 2/3 (Arp2/3) complex which generates new branches from the sides of pre-existing filaments resulting in a highly branched actin network (Machesky et al., 1999; Mullins et al., 1997; Suraneni et al., 2012; Svitkina and Borisy, 1999). It is the addition of actin subunits (G-actin), spread across the entire expanse of the lamellipodia that leads to protrusion of this organelle. The Arp2/3 complex must be activated by proteins known as nucleation promoting factors (NPFs) in order to nucleate filaments (Machesky et al., 1999; Prehoda et al., 2000; Zalevsky et al., 2001). NPFs have been divided into two types: the WASP/N-WASP and the SCAR/WAVE family of proteins comprising type 1 NPFs, and Cortactin and the closely related hematopoetic-specific protein-1 (HS1) comprising type II (Goley and Welch, 2006). While type I NFPs generally bind and activate Arp2/3 via a shared VCA (verprolin homology, central, acidic) region, Cortactin and HS1 use an N-terminal acidic region (NtA) (Goley and Welch, 2006; Weaver et al., 2001).

Cortactin, unlike type I NPFs, can be found integrated within the lamellipodia. Data from FRAP analysis suggests that it recovers throughout the organelle after photobleaching rather than just at the leading edge (Lai et al., 2008). Cortactin can bind to both the sides of actin filaments and at Arp2/3 generated branch junctions where it is thought to stabilize them (Weaver et al., 2001). Interestingly, *in vitro* single molecule experiments determined that Cortactin has a ~300 fold increased affinity for branch junctions over the sides of actin filaments suggesting the protein preferentially targets these sites (Helgeson and Nolen, 2013). Type I NPFs are more potent activators of the Arp2/3 complex than Cortactin, however, the addition of Cortactin to GST-VCA beads increased bead motility, suggesting that Cortactin may synergize with type I NPFs during filament nucleation (Helgeson and Nolen, 2013; Siton et al., 2011;

70 Weaver et al., 2002). Previously, it had been shown that Cortactin competes with the VCA

71 domain for binding to the Arp3 subunit of the Arp2/3 complex, and more recently single

72 molecule experiments from Helgeson and Nolen demonstrate that Cortactin replaces the VCA

73 domain of type I NPFs during nucleation (Helgeson and Nolen, 2013; Weaver et al., 2001).

74 Thus, it appears that Cortactin both stimulates the formation of branches while simultaneously

75 stabilizing them. This type of synergy may allow for continued dendritic nucleation while

76 preventing the potential stalls caused by the tight membrane association of type 1 NPFs

77 (Helgeson and Nolen, 2013). An examination of this synergy between type I and type II NPFs

78 remains to be fully investigated *in vivo,* thus it is unclear how it fits into the paradigm of

79 lamellipodial protrusion and cell migration.

80   Overexpression of Cortactin has been associated with increased metastasis and

81 invasion in a host of cancers from breast carcinomas, and head and neck squamous cell

82 carcinomas, to melanoma, colorectal cancers, and glioblastomas (Åkervall et al., 1995; Buday

83 and Downward, 2007; Hirakawa et al., 2009; Kirkbride et al., 2011; Rothschild et al., 2006;

84 Weaver, 2008; Xu et al., 2010). In support of this, overexpression of Cortactin in NIH 3T3 cells

85 led to an increase in motility and invasiveness. Similarly, overexpression of Cortactin in breast

86 cancer cells led to increased metastasis in nude mice (Patel et al., 1998). RNAi experiments in

87 HT1080 cells suggest that Cortactin enhances lamellipodial persistence, and both the Arp2/3

88 and F-actin binding sites of Cortactin were required for this persistence (Bryce et al., 2005).

89 Cortactin depletion also led to a decrease in the rate of adhesion formation, however, given the

90 importance of the lamellipodia to the formation of nascent adhesions, it may be difficult to

91 uncouple these phenotypes (Bryce et al., 2005; Wu et al., 2012).

92   Cortactin also localizes to other parts of the cell where dynamic actin assembly occurs

93 including endosomes, podosomes, invadopodia, and the dendritic spines of neurons (Ammer

94 and Weed, 2008; Buday and Downward, 2007; MacGrath and Koleske, 2012; Ren et al., 2009).

95 Coincident with Cortactin at some of these sites of dynamic actin are two Cortactin binding

96 proteins, Cortactin Binding Protein 2 (CTTNBP2) and Cortactin Binding Protein N-terminal like

97 (CTTNBP2NL or CortBP2NL).

98   Human CTTNBP2, coded for by the *CTTNBP2* gene, is found primarily in neurons.

99 CTTNBP2 interacts with the C-terminal SH3 domain of Cortactin (Ohoka and Takai, 1998) and

100 previous studies have demonstrated that CTTNBP2 co-localizes with both Cortactin and actin at

101 the lamellipodia. CTTNBP2 depletion in rat hippocampal neurons decreased the width and

102 density of dendritic spines, suggesting that CTTNBP2 plays a role alongside with Cortactin in

103 dendritic spine maintenance (Chen and Hsueh, 2012). Additionally, before dendritic spine

3

104   formation, CTTNBP2 associates with microtubules through its central region and oligomerizes

105   through its N-terminal region coiled-coil motif. CTTNBP2 oligomers bound to microtubules

106   promotes microtubule bundle formation and tubulin acetylation (Shih et al., 2014).

107   Much less is known about CTTNBP2NL, and a clear cellular function for the protein has

108   yet to be fully elucidated. CTTNBP2NL is found in epithelial, spleen, and liver cells and unlike

109   CTTNBP2, CTTNBP2NL does not associate at the cell cortex, but instead can be found on actin

110   stress fibers where it can redistribute Cortactin to these structures (Chen et al., 2012).

111   Interestingly, in rat hippocampal neurons, exogenous CTTNBP2NL is unable to rescue the

112   effects of CTTNBP2 depletion on dendritic spine morphology (Chen et al., 2012), indicating that

113   the two proteins are not functionally similar in the context of mammalian dendritic spine

114   morphology. Given Cortactin's widespread expression, CTTNBP2NL may very well play

115   important roles in other dynamic actin-based structures in non-neuronal cell types.

116   Drosophila CG10915 is an uncharacterized protein-coding gene that shows amino acid

117   sequence similarity to CTTNBP2 and CTTNBP2NL. CG10915 is expressed ubiquitously

118   throughout the larval and adult fly, with higher expression levels in the central nervous system

119   and ovaries (Gelbart and Emmert, 2013). Here, we investigate the role of CG10915 in

120   *Drosophila* to determine its role in actin dynamics. We demonstrate that the *Drosophila* gene

121   CG10915 (hereafter referred to as *Nausicaa (naus)*) alters lamellipodial and protrusive actin

122   dynamics in migratory cells and neurons in a Cortactin-dependent manner.

123

124

125

126 **Results.**

127 Bioinformatic queries initially indicated that the *Drosophila* CG10915 locus at cytological position

128 55B9, was a potential homolog of human Filamin-A interacting protein (FILIP) due to it sharing

129 approximately 20 percent identity. Upon further refinement of these queries (Clustal Omega

130 Multiple Sequence Alignment, Goujon et al., 2010; Sievers et al., 2011) we found that CG10915

131 is more similar to both human Cortactin Binding Protein 2 N-terminal like (CTTNBP2NL) and

132 Cortactin Binding Protein 2 (CTTNBP2) sharing approximately 30 percent and 28 percent

133 identity, respectively (Supplemental Figure 1). We have subsequently named CG10915, the

134 putative *Drosophila* homolog of CTTNBP2 and CTTNBP2NL, *nausicaa* (*naus*), after the

135 princess in Homer's *The Odyssey* who helps to ensure Odysseus's safe passage home from

136 Phaeacia. *Naus* has two splice variants, each encoding a polypeptide of 609 amino acids. The

137 highest degree of conservation between Naus, CTTNBP2, and CTTNBP2NL occurs in the

138 coiled-coil motif found within the N-terminal Cortactin binding protein (CortBP2) domain.

139 Furthermore, the three proteins also share a highly conserved proline-rich patch located near

140 their C-termini that has been shown to facilitate the interaction between Cortactin and CTTNBP2

141 in COS cells (Supplemental Figure 1) (Chen et al., 2012).

142

143 *Nausicaa localizes to lamellipodia of S2R+ cells in a Cortactin-dependent manner.*

144 We first assessed the localization of EGFP-tagged Naus by live-cell imaging of *Drosophila*

145 S2R+ cells using total internal reflection fluorescence (TIRF) microscopy (Figure 1A,

146 Supplemental Video 1). Interestingly, we observed an enrichment of Naus in the circumferential

147 lamellipodia of these cells which persisted following fixation (data not shown) and when we

148 extracted the cells with detergent prior to fixation (Figure 1B). We next investigated whether

149 Naus localized to other actin-based structures. *Drosophila* S2R+ cells do not form prominent

150 stress fibers, however, ML-DmD25c2 (D25) cells which are derived from third instar imaginal

151 wing discs, readily form these structures. We co-expressed EGFP-tagged Naus with mCherry-

152 Alpha-actinin to mark stress fibers and actin bundles, and observed Naus weakly localizing to

153 these structures as well (Supplemental Figure 2A). Furthermore, much like our results from

154 S2R+ cells, we also observed lamellipodial enrichment of Naus in D25 cells (Supplemental

155 Figure 2B). Interestingly, while CTTNBP2NL can also be found co-localizing to microtubules in

156 COS cells (Chen et al., 2012), we failed to observe any colocalization between Naus and

157 microtubules in either S2R+ or D25 cells under these conditions (data not shown). Collectively,

158 these results suggest that Naus behaves similarly to both CTTNBP2 and CTTNBP2NL,

159 localizing to both the lamellipodia and bundled actin structures.

5

160

161   Given the potential interaction between Naus and *Drosophila* Cortactin (CG3637), we next

162   tested whether this lamellipodial enrichment in S2R+ cells is Cortactin-dependent. While it has

163   been demonstrated that mammalian CTTNBP2 and CTTNBP2NL interacts with Cortactin, the

164   role Cortactin plays in this interaction is unclear. Using two independent dsRNA sequences we

165   depleted Cortactin and expressed EGFP-tagged Naus and observed a distinct loss on Naus'

166   lamellipodial localization (Figure 1C, and Supplemental Video 1). This loss in enrichment was

167   even more evident in cells that were detergent extracted prior to fixation (Figure 1D). Line-scan

168   analysis, where we compared control RNAi treated cells to cell treated with either Cortactin

169   dsRNAs or in combination, further corroborated this change in localization (Figure 1E). To

170   quantify this change, we used Mander's Coefficient and measured the fraction of Naus

171   overlapping with F-actin (stained by fluorescently labeled phalloidin) following Cortactin

172   depletion, and found a statistically significant decrease in the amount of Naus overlapping with

173   actin further supporting that Naus' association with actin cytoskeleton is Cortactin-dependent

174   (Bolte and Cordelières, 2006) (Figure 1G & H). This differs from CTTNBP2 where upon

175   Cortactin re-distribution, CTTNBP2 does not re-localize in neurons suggesting a Cortactin-

176   independent mechanism of localization for this potential Naus homolog (Chen and Hseuh,

177   2012). Given that Cortactin interacts with Arp2/3 complex at the lamellipodia (Uruno et al.,

178   2001), we depleted the p20 subunit of Arp2/3 complex by RNAi and observed a similar loss of

179   localization (Supplemental Figure 3). Collectively, these results suggest that Naus is enriched in

180   the lamellipodia and that this enrichment to actin structures is Cortactin-dependent.

181

182   Given that Naus' lamellipodial localization is Cortactin-dependent, we next wanted to

183   characterize the relationship between the two proteins. We co-expressed Naus-EGFP with myc-

184   tagged Cortactin in S2R+ cells and again used Mander's Coefficient to determine the degree of

185   overlap between these proteins (Figure 2A, B, & D). The Mander's Coefficient revealed that just

186   over 50% of myc-Cortactin overlapped with Naus while nearly 80% of Naus-EGFP overlapped

187   with Cortactin. This asymmetry in co-localization, which was statistically significant (Student's t-

188   test, p-value <0.0001), suggests that while not all of the Cortactin in the cell is associated with

189   Naus, the majority of the Naus in the cell can be found overlapping with Cortactin. This

190   supports the hypothesis that Naus relies on Cortactin for proper localization. Naus, like

191   CTTNBP2 and CTTNBP2NL, has a proline rich patch (PPPIP) that was previously shown to be

192   required for Cortactin binding (Supplemental Figure 1) (Chen et al., 2012). To further elucidate

193   the relationship between Naus and *Drosophila* Cortactin we mutated these proline residues

6

194   (amino acid positions 563-567) to alanine and expressed an EGFP-tagged version (Naus-

195   AAAIA) in S2R+ cells (Figure 2C). Our initial observations indicated that rather than a specific

196   localization to actin-based structures, Naus-AAAIA appeared to be distributed non-specifically

197   throughout the cell a pattern similar to what we observe when we expressed untagged-EGFP in

198   these cells (Figure 2C & E). Line-scan analysis corroborates this observation and reveals a

199   distinct loss in lamellipodial-enriched Naus when these residues are mutated (Figure 2F). This

200   loss is similar to the loss of lamellipodial enrichment we observed following Cortactin RNAi

201   (Figure 1C). When we quantified the amount of colocalization by Mander's Coefficient we

202   observed a statistically significant decrease in the amount of overlap between Naus-AAAIA and

203   Cortactin further supporting the observation that this proline patch is facilitating the interaction

204   between Naus and Cortactin (Figure 2B & D). Similar to what we observed in S2R+ cells,

205   EGFP-tagged Naus-AAAIA failed to localize specifically to actin structures in D25 cells

206   (Supplemental Figure 2C). These results suggest that Naus, like its mammalian counterparts,

207   interacts with Cortactin through this conserved proline patch, but uniquely, requires Cortactin for

208   proper localization. Interestingly, while we failed to observe microtubule localization in cells

209   expressing wild-type EGFP-Naus, on occasion we did observe EGFP-tagged Naus-AAAIA

210   colocalizing with microtubules in both S2R+ and D25 cells (Supplemental Figure 2D). It is likely

211   that under conditions where its affinity for Cortactin is reduced, Naus may bind microtubules.

212   While more detailed analysis of this microtubule localization is needed, we feel that this is

213   beyond the scope of this current study.

214

215   Given this dependence on Cortactin for its lamellipodial localization, we next sought to

216   determine if Naus' dynamics are altered in the absence of Cortactin. We first used

217   Permeabilization Activated Reduction in Fluorescence (PARF) to measure the loss of Naus-

218   EGFP fluorescence following control or Cortactin RNAi treatments (Figure 3). PARF uses a low

219   concentration of digitonin to gently permeabilize cells which leads to a large-scale dilution of the

220   unbound pool of protein and a disruption of the initial equilibrium of the bound protein. The

221   subsequent decrease in fluorescence can be fit to an exponential model and can be used to

222   calculate a $t_{1/2}$ for fluorescence loss of the bound fraction (Singh et al., 2016). Cortactin

223   depletion led to a rapid loss in Naus-EGFP fluorescence following permeabilization with an

224   average half-time of 5.956 ± 0.8s while control RNAi treated cells had an average half-time of

225   fluorescence decay of 11.28 ± 2.1s, nearly double that of Cortactin depleted cells (Figure 3A-B

226   & E-F, Supplemental Videos 2-3). These results suggest that depletion of Cortactin leaves a

227   larger portion of the Naus pool free to quickly diffuse out of the cell rather than maintaining an

7

228   association with Cortactin and the actin cytoskeleton. To corroborate our PARF results, we also

229   performed Fluorescence Recovery After Photobleaching (FRAP) in cells treated with control or

230   Cortactin RNAi. Again, we found that depletion of Cortactin led to a decrease in the half-time of

231   recovery, from 56.5 ± 12.2s in control cells to 24.7 ± 4.9s in Cortactin depleted cells (Figure 3C-

232   D & G-H, Video 4). Similar to our PARF results, our FRAP experiments suggest that in the

233   presence of Cortactin, Naus is more stably associated with the cytoskeleton leading to a slower

234   half-time of recovery as compared to Cortactin depleted cells. Collectively, these results

235   indicate that Cortactin may function as an anchor, helping Naus maintain lamellipodial

236   localization.

237

238   While our results indicate that Cortactin affects Naus' dynamics, we wanted to determine if the

239   inverse is also true. Once again, we used PARF, this time to measure the loss of Cortactin

240   fluorescence following RNAi depletion of Naus (Figure 4A & B). This analysis revealed that

241   depletion of Naus led to a statistically significant decrease in the half-time Cortactin's

242   fluorescence decay as compared to control RNAi treated samples (Figure 4C & D,

243   Supplemental Videos 5-6). The average half-time of fluorescence decay for mCherry-Cortactin

244   following Naus depletion was 15.32 ± 1.3 s, while the fluorescent decay in control treated cells

245   was 20.13 ± 1.6 s (Figure 4C). A similar increase in Cortactin's mobility was found in the

246   dendritic spines of rat primary hippocampal neurons depleted of CTTNBP2 following FRAP

247   analysis (Chen et al., 2012).

248

249   *Depletion of Nausicaa alters lamellipodial actin dynamics.*

250   Cortactin can function as both a type II nucleating promoting factor (NPF) and a

251   stabilizer of Arp2/3 generated actin branches. Any changes to its dynamics could affect actin

252   polymerization, branch density, and the overall rates of lamellipodial protrusion (Ammer and

253   Weed, 2008; Bryce et al., 2005; Uruno et al., 2003; Weaver et al., 2001). Additionally,

254   mammalian CTTNBP2 is known to regulate dendritic spine formation, which are Arp2/3-

255   nucleated actin-rich structures (Chen et al. 2012), though the direct effect on actin dynamics

256   and architecture is unexplored. Given the putative role Naus plays in regulating Cortactin

257   dynamics, we sought to determine if Naus plays a role in regulating lamellipodial actin

258   dynamics. We first depleted Naus in S2R+ cells and examined the circumferential lamellipodia

259   of these cells by quantitative fluorescence microscopy (Figure 5A-D). Using phalloidin to

260   measure F-actin we performed line-scan analysis as well as quantified the mean actin density of

261   the lamellipodia (Figure 5C & D). Our analysis revealed an increase in actin fluorescence in the

262   lamellipodia following Naus depletion which was statistically significant (p-value < 0.001,

263   Student's t-test, n= 30 cells per condition) when compared to control RNAi treated cells

264   prepared in parallel (Figure 5D).

265   As this increase in filamentous actin likely implies a change in dynamics, we next asked

266   if depletion of Naus leads to changes in the rates of actin retrograde flow. Actin retrograde flow

267   in the lamellipodia is the result of a combination of the plasma membrane pushing back against

268   the force of actin polymerization and non-muscle myosin II contractility. Given Naus'

269   lamellipodial localization and its association with Cortactin, it is likely that any changes we

270   observe in actin retrograde flow are due to changes in actin polymerization rather than

271   contractility. To measure actin retrograde flow we turned to Quantitative Fluorescence Speckle

272   Microscopy (QFSM) (Danuser and Waterman-Storer, 2006). Following treatment with Naus or

273   control RNAi, we transfected S2R+ cells with EGFP-tagged actin using a copper-inducible

274   promoter which allowed us to closely regulate the level of expression (Iwasa and Mullins, 2007).

275   We imaged the cells by TIRF microscopy and analyzed the resulting movies using a Matlab-

276   based program, QFSM, developed by the Danuser lab (Figure 5E & F, Supplemental Video 7)

277   (Mendoza et al., 2012). Interestingly, Naus depletion led to a statistically significant 1.4-fold (p-

278   value = 0.0151, Student's t-test, n = 40 cells and 46 cell for control and Naus RNAi,

279   respectively) decrease in actin retrograde flow speeds in the lamellipodia as compared to

280   control RNAi treated cells (Figure 5G). We measured the mean fluorescence intensity of EGFP-

281   actin in these cells to determine if actin expression levels were dictating the speed of retrograde

282   flow and found no statistically significant difference between the two RNAi conditions (Figure

283   5H). This slowing of actin dynamics in combination with an increase in F-actin in the

284   lamellipodia indicates that Naus helps to regulate actin branch dynamics, likely through its

285   interaction with Cortactin.

286

287   *Depletion of Nausicaa leads to an increase in the number of long, unbranched actin filaments*

288   *the lamellipodia.*

289   The decrease in the rate of actin polymerization coupled with the increase in filamentous

290   actin we observed in the lamellipodia of Naus depleted S2R+ cells suggests that Naus may play

291   a role in the regulating the fundamental architecture the actin cytoskeleton. To test this, we

292   turned to platinum replica electron microscopy (Svitkina, T., 2016). We generated platinum

293   replicas of control and Naus depleted S2R+ cells and imaged the actin cytoskeleton of the

294   lamellipodia using electron microscopy (Figure 6). Interestingly, while the lamellipodia of control

295   treated cells remained highly branched, typical of an Arp2/3 nucleated dendritic network (Figure

9

296 6A & B), the lamellipodia of Naus depleted cells was composed of extremely long, unbranched

297 filaments with very few branch junctions (Figure 6C & D). Curiously, the ultrastructure of Naus

298 depleted lamellipodia were reminiscent of the lamellipodia of Rat2 cells following the membrane

299 targeting of Ena/VASP proteins (Bear et al. 2002), and suggest that in the absence of Naus

300 there is either reduction in barbed-end capping or branching. Given that Cortactin is both an

301 NPF and can stabilize the Arp2/3 complex at branch junctions, these long, unbranched

302 filaments we observed are likely the result of a reduction in Cortactin's activity. Without the

303 stabilization provided by Naus, Cortactin fails to remain associated with Arp2/3 branches

304 ultimately leading to reductions in actin polymerization and branch formation. Furthermore,

305 these data assert a novel role for Naus in the regulation of the lamellipodial machinery and likely

306 has broader implications in the way this actin-based protrusive organelle functions during cell

307 migration.

308

309 *Depletion of Nausicca leads to a decrease in cell migration and directionality.*

310   Actin polymerization is the main engine behind lamellipodial protrusion and ultimately,

311 cell migration. Given the alterations to both actin dynamics and architecture we observed

312 following Naus depletion, we next sought to determine whether Naus plays a role in cell

313 migration. To do this, we performed a random cell migration assay where we treated D25 cells

314 with control or Naus RNAi for seven days, plated them on mixture extracellular matrix (ECM),

315 and imaged them by phase-contrast microscopy for six hours (Figure 7A-D, Supplemental Video

316 8). Cells were then manually tracked yielding migration speeds. In comparing the instantaneous

317 velocity of approximately 50 cells per condition we found that depletion of Naus led to a modest

318 but statistically significant decrease in the speed of cell migration. Control RNAi cells migrated

319 at an average rate of approximately 1.6 ± 0.09 µm min^{-1} while Naus depleted cells migrated at

320 an average rate of 1.4 ± 0.05 µm min^{-1}(p-value < 0.0001, Student's t-test) (Figure 7E). Cells

321 undergoing random migration still maintain a degree of directionality. When we measured the

322 directionality of Naus depleted cells we found they were statistically significantly less directional

323 than Control RNAi treated cells. Where a value of 1.0 is completely directional, Control RNAi

324 treated cells showed a value of 0.7 ± 0.07 a.u. while Naus depleted cells were 0.5 ± 0.04 a.u.

325 (p= 0.0230, Student's t-test) (Figure 7F). Directional persistence is a function of actin branch

326 density and increases to actin branching positively correlates with the directionality of randomly

327 migrating cells (Harms et al., 2005). Thus, the decrease in directionality we observed in Naus

328 depleted D25 cells is consistent with the ultrastructural data gathered from S2R+ cells.

329   While these results suggest that Naus plays a role in maintaining both the speed and the
330   directionality of migrating cells we wanted the further explore how Naus regulates the
331   lamellipodial dynamics that govern cell migration. Using kymographs taken from phase-contrast
332   microscopy movies we measured lamellipodial persistence, the speeds of protrusion and
333   retraction, the frequency of protrusions, and the amplitude of protrusions (Figure 7B & D) (Bear
334   et al., 2002; Hinz et al., 1999). Despite the slower rates of cell migration, Naus depleted cells
335   had longer lamellipodial protrusions that persisted for greater periods of time as compared to
336   control RNAi treated cells. The average maximum length of lamellipodial protrusions (the
337   amplitude of protrusions) for Naus depleted D25 cells was 3.4 ± 0.21 µm which is statistically
338   significantly greater than control cells at 2.8 ± 0.18 µm (p=0.0265, Student's t-test) (Figure 7G).
339   This data corroborates our ultrastructural data in S2R+ cells and suggests the lamellipodia of
340   Naus depleted D25 cells may also contain longer, unbranched filaments. Interestingly, unlike
341   the less persistent lamellipodia of cells where Ena/VASP proteins were membrane targeted, we
342   observed an increase in persistence following Naus depletion, from 85.8 ± 6.0 s in control RNAi
343   treated cells to 116 ± 11.0 s in Naus RNAi treated cells (p=0.025, Student's t-test) (Figure 7H).
344   This suggests that despite have long, unbranched filaments, the lamellipodia of Naus depleted
345   cells are still able to protrude without an increase in buckling. Depletion of Naus had a specific
346   effect on lamellipodial dynamics and other parameters such as the frequency of protrusions, the
347   speed of protrusions and retractions, and the total distance the cells migrated over a two-hour
348   period remain unchanged as compared to control RNAi treated D25 cells (Supplemental Figure
349   4). Collectively, we found that Naus depletion in D25 cells led to an increase lamellipodial
350   persistence while simultaneously decreasing cell migration speeds and directionality.
351
352   *Depletion of Nausicaa decreases the number of branches in Drosophila larval neurons.*
353   This fine-tuning of actin dynamics is not only critical to the function of lamellipodia, but
354   plays a major role in the morphology and function of other dynamic actin structures. One actin
355   based-structure that is particularly sensitive to changes in actin dynamics are dendritic spines
356   (Fischer et al., 1998; Hotulainen and Hoogenraad, 2010; Matus, 2000). Accordingly, we sought
357   to determine whether Naus also plays a role in morphology of *Drosophila* neurons. While it
358   remains controversial whether *Drosophila* neurons form dendritic spines *in vitro* we focused on
359   the overall neuronal morphology of third instar larvae neurons in culture. Using the UAS-Gal4
360   system, we depleted Naus specifically in neurons using the pan-neuronal Gal4 driver Elav. The
361   brains of third instar larvae were removed and enzymatically dissociated. The resulting
362   neuroblasts were allowed to differentiate in culture for 24 hours (Lu et al., 2013) (Figure 8A-C).

11

363   Following fixation and staining with the neuronal marker Futsch, the morphology of the neurons

364   was assessed using Sholl analysis (Ferreira et al., 2014; Sholl, 1953). Sholl analysis analyzes

365   the neuronal morphology by counting the number of intersections for concentric circles from the

366   center of the cell body. Interestingly, we observed a distinct difference in the Sholl profiles of

367   Naus depleted neurons as compared to control neurons prepared in parallel, suggesting a

368   difference in neuronal arborization (Figure 8D). Similarly, the maximum Sholl radius in which

369   neuronal intersections were still detected was significantly lower in Naus depleted neurons

370   (Figure 8E). Consistent with this result, when neuron 2D skeletons were analyzed with ImageJ

371   Simple Neurite Tracer (Longair et al., 2011), we observed that Naus depleted neurons showed

372   decreased average branch length in comparison to controls (Figure 8F &G). Taken together,

373   these results suggest that Naus plays a role in neuronal branch arborization and branch length.

374

375 **Discussion.**

376 The formation of actin protrusive structures such as the lamellipodia of migrating cells and the

377 dendritic spines of neurons rely on Arp2/3 generated actin branches. Changes to the density

378 and stability of actin branches can affect the overall morphology of these structures and

379 ultimately, their function. We are interested in proteins that play a role in this fine-tuning of actin

380 branches such as the type II NPF and actin branch stabilizer, Cortactin. Here we characterize

381 Nausicaa, a putative *Drosophila* homolog of two mammalian Cortactin binding proteins,

382 CTTNBP2 and CTTNBP2NL. Using cultured and primary *Drosophila* cells we demonstrate that

383 Naus, through its interaction with Cortactin, regulates actin-branch dynamics, lamellipodial

384 protrusion, and the morphology of neurons.

385

386 *Nausicca is likely the fly homolog of both CTTNBP2 and CTTNBP2NL*

387 We described a previously uncharacterized protein encoding gene *cg10915*, which we have

388 subsequently named *nausicaa (naus)*. While bioinformatic queries indicate the *naus* is more

389 closely related to mammalian CTTNBP2NL than CTTNBP2, based on its localization and

390 putative role in regulating the morphology of neurons, we argue that Naus covers the function

391 for both proteins in flies. We do not have to look much further for another example of this

392 refinement of the *Drosophila* genome then the Ena/VASP family of proteins. While there are

393 three of these critical regulators of the actin cytoskeleton in a typical mammalian genome,

394 mammalian ena or Mena, VASP, and EVL (Ena/VASP-like), the fly genome only contains one,

395 Enabled (Ena). It is interesting to speculate that the mammalian homologs could be the result of

396 a gene duplication event of an ancestral gene that is similar to *naus.*

397

398 *Nausicca's lamellipodial enrichment is Cortactin dependent*

399 We used TIRF microscopy of both fixed and live cells in combination with RNAi treatments and

400 point mutations and determined that Naus' lamellipodial enrichment, is Cortactin dependent.

401 Using two different RNAi sequences targeting Cortactin, we found that depletion of Cortactin

402 leads to a loss of Naus localization at actin structures. This differs from the mammalian

403 counterpart in which re-localization of Cortactin by glutamate stimulation in neurons does not

404 lead to CTTNBP2 redistribution. We observed a similar loss in localization upon expression of a

405 point mutant where the proline residues in the conserved proline patch (Supplemental Figure 1)

406 were mutated to alanine (amino acid positions 563-567). Thus Naus, like its mammalian

407 counterparts, uses this same conserved region for its association with Cortactin. Along with

408 abolishing the interaction with Cortactin in COS cells, a similar proline mutant of rat CTTNBP2

13

409   failed to rescue the decrease in dendritic spine density following depletion of endogenous

410   CTTNBP2 (Chen et al., 2012), arguing that not only is this association important for proper

411   localization, but it is also needed for proper function.

412

413   *Nausicaa and Cortactin regulate one another's dynamics in a reciprocal manner*

414   Our kinetic studies of Naus and Cortactin reveal a mutual relationship between the two proteins.

415   By both FRAP and Permeabilization Activated Reduction in Fluorescence (PARF), we found

416   that following Cortactin RNAi, Naus was no longer anchored to the actin cytoskeleton. This

417   kinetic data supports our localization studies and further implicates Cortactin's role in recruiting

418   Naus to the cytoskeleton. Cortactin is incorporated throughout the lamellipodia where it likely

419   targets nascent actin branch junctions having a 300-fold increased affinity for junctions over the

420   sides actin filaments. Interestingly, using *in vitro* single molecule imaging, Helgeson and Nolen

421   observed that Cortactin's average lifetime at existing branch junctions during active branching

422   was 29.5 s (Helgeson and Nolen, 2013), while the lifetime of branches *in vitro* has been

423   observed to be between 8 and 27 minutes (Mahaffy and Pollard, 2006; Martin et al., 2006). Our

424   kinetic data (Figure 4) suggests that Naus may function to retain Cortactin throughout the

425   lamellipodia, likely at branch junctions given Cortactin's high affinity for these sites. While this

426   increase in the time at junctions may not be on par with the reported lifetimes *in vitro*,

427   lamellipodial actin undergoes treadmilling. Thus, this delay in the dissociation of Cortactin as a

428   result of its association with Naus may be more consequential *in vivo*. Delays in Cortactin's

429   dissociation could also lead to a decrease in the number of new branches given its ability to

430   function as a type II NPF. Furthermore, while outside the scope of this study, it would be

431   interesting to determine how Naus affects the activity of de-branching enzymes such as cofilin

432   or GMF given Naus' putative role in regulating branch formation and dynamics.

433

434   *Naussica regulates branch density, actin-retrograde flow rates, and lamellipodial protrusion.*

435   Actin retrograde flow is the result of both contractility generated by non-muscle myosin II and

436   the force of the cell membrane pushing back against actin filaments as they polymerize.

437   Quantitative fluorescence speckle microscopy revealed that depletion of Naus leads to a

438   decrease in actin retrograde flow speeds within the lamellipodia (Figure 3). This decrease in

439   retrograde flow may be the result of an overall decrease in Arp2/3 nucleation and branch

440   junction stabilization. Two critical observations led us to this hypothesis. Firstly, our kinetic data

441   indicates Cortactin more readily dissociates from the actin cytoskeleton following Naus

442   depletion. Secondly, we found that RNAi depletion of Naus led to an increase in actin in the

14

443   number of long, unbranched actin filaments by platinum replica electron microscopy (Figure 6).

444   Thus, Cortactin could be undergoing a cycle of precocious dissociation from branch junctions

445   leading to less activation of the Arp2/3 complex and a decrease in the stability of branched

446   junctions. This putative mechanism draws parallels to what has been observed in fibroblasts

447   lacking Ena/VASP proteins (Bear et al., 2002). The lamellipodia of fibroblast where Ena/VASP

448   proteins were miss-targeted to the cell membrane and contained longer, less branched actin

449   filaments. These changes to the actin architecture resulted also affected the dynamics of the

450   lamellipodia. The longer, less branched actin filaments decreased the speed of cell migration

451   and the directionality of this migration but increased the amplitude of lamellipodial protrusions

452   and increased lamellipodial persistence (Figure 7). Interestingly, depletion of Cortactin also led

453   to a decrease in random cell motility, however these cells had less persistent lamellipodial

454   protrusions suggesting nuanced differences between the loss of Cortactin and the loss of Naus

455   to actin dynamics (Bryce et al., 2005). These differences may very well lie in function of Naus to

456   stabilize Cortactin retaining it in the lamellipodia. Naus depletion appears to differ somewhat

457   from the depletion of the branch destabilizer Coronin 1B as well. The depletion of Coronin 1B

458   leads to a more densely branched actin network and a decrease in retrograde flow rates.

459   Coronin 1B depletion also leads to an increase the speeds of lamellipodial protrusion while

460   reducing lamellipodial persistence (Cai et al., 2007; Hostos et al., 1993; Krause and Gautreau,

461   2014). Thus, Naus' role in fine tuning the lamellipodia is distinct from that of both Cortactin and

462   Coronin 1B.

463

464   *Naussica plays a role in regulating neuronal morphology*

465   This role in regulating actin dynamics also plays out in determining the morphology of neurons.

466   Using fly genetics we depleted Naus in neuroblasts, which differentiate into neurons in culture.

467   We found that depletion of Naus led to a decrease in the number of processes made in

468   comparison to wild-type neurons (Figure 8). Similarly, depletion of CTTNBP2 also led to a

469   decrease in neuronal arborization as well as a decrease in the density of dendritic spines (Chen

470   and Hsueh, 2012; Chen et al., 2012; Shih et al., 2014). However, CTTNBP2 also promotes

471   microtubule stability, thus its role in promoting neuronal arborization may have diverged from its

472   role in regulating Cortactin dynamics (Shih et al., 2014). Interestingly, we did not observe wild-

473   type Naus associating with microtubules and it was only upon expression of the alanine mutant

474   (Naus-AAAIA, Supplemental Figure 2D), albeit on a rare occasion, did we observe co-

475   localization with microtubules. Understanding the differences between Naus and CTTNBP2 will

476   likely be the focus of future studies, in particular if they both contribute to the morphology of

477   neurons in distinct ways despite being closely related.

478

479   *Working model for Nausicaa's role in branch nucleation, stabilization and the fine-tuning of the*

480   *lamellipodia*

481   Given the observations detailed here, we propose a model wherein Nausicaa acts through the

482   stabilization of Cortactin at Arp2/3 generated branches to regulate their dynamics (Figure 9). By

483   stabilizing Cortactin, Naus inhibits its precocious dissociation while preventing debranching.

484   Without Naus, Cortactin more freely dissociates from Arp2/3 generated branches leading to the

485   loss of destabilization of branch junctions and an overall decrease in actin branch density

486   throughout the lamellipodia. This decreased density leads to larger scale cellular changes, such

487   as reduced speeds in cell migration (Figure 7) and decreased neuronal branches observed in

488   this study (Figure 8). In a similar manner, Cortactin maintains Naus at the lamellipodia, and

489   when Cortactin is absent, Naus loses this enrichment and, in extremely rare cases, relocalizes

490   to other structures such as microtubules. Collectively, both Naus and Cortactin act in concert to

491   ensure the appropriate spatial and temporal regulation of lamellipodial actin dynamics.

492

493

16

494   **Materials and Methods.**

495

496   *Cell Culture and RNAi*

497   Drosophila S2R+ cell culture and RNAi were performed as described in Rogers and Rogers,

498   2008 and Applewhite et al., 2016. Briefly, S2R+ (Drosophila Genomics Resource Center,

499   Bloomington, IN) cells were cultured in Shields and Sanger media (Sigma-Aldrich, St. Louis,

500   MO) supplemented with 100X antibiotic-antimycotic (Thermo Fisher Scientific, Waltham, MA),

501   and 10% fetal bovine serum (Thermo Fisher Scientific, Waltham, MA) maintained at 25°C.

502   RNAi was administered in six-well plates by treating cells (approximately 50% confluent) with 10

503   µg of double-stranded RNA (dsRNA) in 1 ml of medium each day for 7 days. Control RNAi was

504   made from dsDNA amplified from pBlueScript vector with no known homology to the *Drosophila*

505   genome. For all other dsRNA targets please see Supplemental Table 1 for primer sequences.

506   *Drosophila* ML-DmD25c2 (D25 cells, Drosophila Genomics Resource Center,

507   Bloomington, IN) were maintained as described in Currie and Rogers, 2011. Briefly, D25 cells

508   were cultured in Schneider's media (Thermo Fisher Scientific, Waltham, MA) supplemented with

509   100X antibiotic-antimycotic (Thermo Fisher Scientific, Waltham, MA), 10% fetal bovine serum

510   (FBS, Thermo Fisher Scientific, Waltham, MA), and 10µg/ml insulin (Thermo Fisher Scientific,

511   Waltham, MA). RNAi regimen was the same as described for S2R+ cells (see above).

512   *Drosophila* primary neuroblasts were harvested and cultured as described in Lu et al.,

513   2013. Briefly, the brains of third instar larvae were dissected in Schneider's media

514   supplemented with 20% FBS, and then enzymatically dissociated with liberase (Roche, Basel,

515   Switzerland) at a final concentration of 0.20-0.25 mg/ml in Modified Dissecting Saline (137 mM

516   NaCl, 5.4 mM KCl, 0.17 NaH_2PO_4 0.22 mM $HKPO_4$ 3.3 mM Glucose, 43.8 mM Sucrose, 9.9 mM

517   Hepes, pH 7.5). The Modified Dissecting Solution was replaced with Schneider's media

518   supplemented with 20% FBS and neuroblasts were plated on ECM harvested from the D25

519   cells (see Currie and Rogers, 2011) and allowed to differentiate for 24 hours at 25°C.

520

521   *Molecular Biology*.

522   The cDNA clones for Nausicaa (CG10915) and Cortactin (CG3637) were obtained from the

523   Drosophila Genomics Resource Center (University of Indiana, Bloomington, IN) and were

524   cloned into pMT or pIZ (Invitrogen) vectors following standard PCR procedures. Nausicaa's

525   conserved Cortactin binding motif (amino acid positions 563-567) were mutated to alanine by

526   site directed mutagenesis.

527

17

528   *Immunofluorescence and Live-cell Imaging.*

529   Cells were prepared for immunofluorescence and live-cell imaging as described in Applewhite et

530   al., 2016. S2R+ cells were plated on concanavalin A-treated coverslips attached to laser cut 35

531   mm-tissue culture dishes with UV-curable adhesive (Norland Products, Cranbury, NJ) in Shields

532   and Sanger media supplemented with 10% FBS and 100X antibiotic-antimycotic for both fixed

533   and live-cell imaging. D25 cells were plated on glass bottom dishes (described above) treated

534   with ECM harvested from the cells as described in Currie and Rogers, 2011. Antibodies used in

535   this study include anti-Myc 9E10 (Developmental Hybridoma Bank, Iowa City, Iowa), anti-Futsch

536   (Developmental Hybridoma Bank, Iowa City, Iowa), anti-alpha tubulin (Developmental

537   Hybridoma Bank, Iowa City, Iowa), and anti-beta tubulin (Developmental Hybridoma Bank, Iowa

538   City, Iowa) diluted 1:200 in a 5% solution of normal goat serum (Sigma-Aldrich) and phosphate-

539   buffered solution with 0.1% Triton x-100 (PBST) (Sigma-Aldrich). Secondary antibodies (Alexa-

540   488 and Alexa 594; Jackson ImmunoResearch, West Grove, PA) and phalloidin (Alexa-488 and

541   Alexa-594; Thermo Fisher Scientific) were used at final dilution of 1:100 in PBST. Hoechst

542   (Thermo Fisher Scientific) was diluted 1:10,000 in PBST. All transfections were carried out

543   using using FuGENE HD (Promega, Madison, WI). Expression of pMT vectors was achieved

544   with 250-500 µM final concentration of copper sulfate unless noted otherwise. Cells were fixed

545   using a 10% solution of Paraformaldehyde (Electron Microscopy Sciences, Hatfield, PA) and

546   PEM buffer (100 mM Pipes, 1 mM EGTA, 1 mM $MgCl_2$). Fixed cells were mounted using Dako

547   anti-fade mounting media (Agilent, Santa Clara, CA). All imaging was performed on a total

548   internal reflection fluorescence (TIRF) system mounted on an inverted microscope (Ti-E, Nikon,

549   Tokyo, Japan) using a 100X/1.49NA oil immersion TIRF objective driven by Nikon Elements

550   software unless noted otherwise. Images were captured using a Orca-Flash 4.0 (Hamamatsu,

551   Hamamatsu, Japan) and were processed for brightness and contrast using ImageJ before

552   analysis.

553

554   *Co-localization Analysis*

555   Co-localization was analyzed by line-scan analysis and Mander's coefficient analysis. For line-

556   scan analysis, a 10 µm line was drawn from the cell edge inward and fluorescence intensity was

557   measured. These values were normalized and then averaged for all cells within that condition.

558   Mander's coefficient analysis was performed using the Just Another Colocalization Program

559   (JACoP) plugin for ImageJ (Bolte and Cordelières, 2006). Briefly, intensity thresholds were

560   manually set for both fluorescence channels and then the fraction of overlap was calculated in

561   each direction.

18

562

563   *Neuroblast Analysis*

564   Neuroblasts were analyzed using the Simple Neurite Tracer and Sholl Analysis plugins in

565   ImageJ (Ferreira et al., 2014; Longair et al., 2011). For Sholl Analysis, neuroblasts were

566   converted to a threshold image. Following, a line from the center of the soma to past the further

567   branch tip was drawn to define the space for analysis. The radius for analysis was set to 2 μm

568   concentric circles and the number of intersections per radius was calculated. Similarly, the max

569   Sholl radius was then extracted by the maximum radius at which the number of intersections

570   was greater than zero. For analysis of average branch length and number of branches using

571   Simple Neurite Tracer, a line skeleton of the neuron image was manually drawn and these

572   values were then calculated using the plugin.

573

574   *Permeabilization Activated Reduction in Fluorescence (PARF)*

575   PARF was performed as described in Singh et al., 2016. Briefly, cells were prepared for live

576   imaging as described above. Time-lapse images were captured with constant exposure at a rate

577   of one frame every two seconds. After 40 seconds (20 frames), digitonin (25 μM final

578   concentration) was added. Cells from the same dish were imaged under the same conditions

579   but without digitonin treatment for use as a photofading due to acquisition (PDA) control.

580   Analysis was performed using ImageJ and GraphPad Prism 6. The area of each region of

581   interest (ROI) was held constant. An ellipse of the background of each movie (control and

582   digitonin treatment) was selected and intensity density was determined for the background in

583   each frame. Photofading due to acquisition (PDA) was determined as previously described in

584   Applewhite et al., 2007. The intensity density was determined for a lamellipodial ROI in the

585   control (no digitonin treatment) movie for each plate. The background intensity was subtracted

586   and change in fluorescence was fit to a one phase exponential decay of the following general

587   equation where I is intensity and k is the photofading factor: $I = e^{-kt} + I_o$. The intensity density of

588   a lamellipodial ROI for digitonin cells was obtained in the same manner. Background intensity

589   was subtracted and the intensity density was then multiplied by e^{kt}. The intensity was

590   normalized for each cell and the data was averaged for each condition. To compare the half-life

591   between conditions for statistical significance, the normalized fluorescence for each cell was fit

592   to a one phase exponential decay and $t_{1/2}$ was determined. These half-life values were

593   averaged in each condition and compared using a Student's t-test.

594

595   *Fluorescence Recovery after Photobleaching (FRAP)*

19

596   FRAP was performed using a Zeiss LSM880 laser-scanning confocal microscope (Jena,

597   Germany). Cells were prepared for live imaging as described above. Time-lapse images were

598   captured every 1.34 seconds. After 50 cycles (65.6 sec), selected regions of the cell were

599   bleached (5 iterations) and the intensity was recorded. Intensity was also recorded for a non-

600   bleached region and a background region of the same size was uses for PDA controls. FRAP

601   analysis was performed as described in Applewhite et al., 2007. The fluorescence intensities in

602   the bleached zone in each frame were measured. The background was subtracted and the

603   intensity was corrected for photofading as described above. The intensity was normalized for

604   each ROI. This corrected intensity was fit to a one phase association. The half-life of recovery

605   was calculated as ln2/k. Values were compared using a Student's t-test.

606

607   *Quantitative Fluorescence Speckled Microscopy (QFSM)*

608   RNAi treatment and transfection was performed as described above. Following transfection,

609   cells were induced with 30µM copper sulfate and incubated overnight. Live cell movies were

610   obtained at 200 ms exposure in 2 sec intervals for 2 min. The resulting movies were analyzed

611   using a previously described Quantitative Fluorescent Speckle Microscopy (QFSM) software in

612   MATLAB (Mendoza et al., 2012). Images were acquired at a rate of 30 frames per minute

613   (130nm/pixel, NA=1.4, 16 bit images). Full cell masks were generated using automatic

614   thresholding (MinMax setting). Flow analysis was performed using the flow tracking setting with

615   6 frame integration window. For cell-wise quantification of lamellipodial flow rates, masks of

616   lamellipodial regions for each cell were generated and the average actin flow rate was

617   calculated for the first 30 seconds of each video (n=27-35 cells / group).

618

619   *Platinum Replica Electron Microscopy*

620   Sample preparation for platinum replica electron microscopy was performed as previously

621   described in Svitkina, T., 2016. Briefly, cells were extracted in Extraction buffer (1% Triton X-

622   100, 2% PEG (MW 35 kDa) in PEM buffer supplemented 2 µM phalloidin), washed with PBS

623   and then fixed with 2% glutaraldehyde (EM grade from Electron Microscopy Sciences, Hatfield,

624   PA) in 0.1 M sodium cacodylate, pH 7.3. Fixed cells were then treated with 0.1% tannic acid and

625   0.2 % uranyl acetate in water, critical-point dried, and coated with platinum and carbon. They

626   were then transferred to EM grids for imaging.

627

628   *Random Cell Migration Assay and Kymography*

20

629   D25 cells were plated at a subconfluent density on ECM coated glass bottom dishes and

630   allowed to attach overnight. Cells were imaged every 5 minutes for 6 hours by phase-contrast

631   microscopy using 40X/0.75NA objective. Individual cells were manually tracked using Manual

632   Tracker (ImageJ). Cell directionality was calculated as a ratio of the direct distance between

633   start and end points (D) to the total path length taken by the cells (T). To measure the rates of

634   lamellipodial protrusion, retraction, persistence, frequency, and amplitude, kymographs were

635   made using the Multi Kymograph ImageJ plugin from phase-contrast movies acquired every 2

636   seconds for 10 minutes. Kymographs were generated from phase-contrast movies of migrating

637   D25 cells acquired every 2 seconds for 10 minutes. A line approximately 16 microns in width

638   was drawn from the center of the cell to a few microns beyond the cell periphery. Following the

639   protocol established by Hinz et al., 1999, these kymographs were used to extract the

640   lamellipodial protrusion parameters. Statistics were performed using GraphPad Prism 7.

641

661

662   **Competing Interests**.

663   The authors declare that there are no competing interests.

664

665

666 **References.**

667 Abercrombie, M., Heaysman, J.E.M., and Pegrum, S.M. (1970). The locomotion of fibroblasts in
668 culture: II "Ruffling." Exp. Cell Res. *60,* 437-444.

669 Åkervall, J.A., Jin, Y., Wennerberg, J.P., Zätterström, U.K., Kjellén, E., Mertens, F., Willén, R.,
670 Mandahl, N., Heim, S., and Mitelman, F. (1995). Chromosomal abnormalities involving 11q13
671 are associated with poor prognosis in patients with squamous cell carcinoma of the head and
672 neck. Cancer *76*, 853–859.

673 Ammer, A.G., and Weed, S.A. (2008). Cortactin Branches Out: Roles in Regulating Protrusive
674 Actin Dynamics. Cell Motil. Cytoskeleton *65*, 687–707.

675 Applewhite, D.A., Barzik, M., Kojima, S., Svitkina, T.M., Gertler, F.B., and Borisy, G.G. (2007).
676 Ena/VASP Proteins Have an Anti-Capping Independent Function in Filopodia Formation. Mol.
677 Biol. Cell *18*, 2579–2591.

678 Applewhite, D.A., Davis, C.A., Griffis, E.R., and Quintero, O.A. (2016). Imaging of the
679 Cytoskeleton Using Live and Fixed Drosophila Tissue Culture Cells. Methods Mol. Biol. Clifton
680 NJ *1365*, 83–97.

681 Bear, J.E., Svitkina, T.M., Krause, M., Schafer, D.A., Loureiro, J.J., Strasser, G.A., Maly, I.V.,
682 Chaga, O.Y., Cooper, J.A., Borisy, G.G., et al. (2002). Antagonism between Ena/VASP proteins
683 and actin filament capping regulates fibroblast motility. Cell *109*, 509–521.

684 Bolte, S., and Cordelières, F. (2006). A guided tour into subcellular colocalization analysis in
685 light microscopy. J. Microsc. *224*, 213–232.

686 Bryce, N.S., Clark, E.S., Leysath, J.L., Currie, J.D., Webb, D.J., and Weaver, A.M. (2005).
687 Cortactin Promotes Cell Motility by Enhancing Lamellipodial Persistence. Curr. Biol. *15*, 1276–
688 1285.

689 Buday, L., and Downward, J. (2007). Roles of cortactin in tumor pathogenesis. Biochim.
690 Biophys. Acta BBA - Rev. Cancer *1775*, 263–273.

691 Cai, L., Marshall, T.W., Uetrecht, A.C., Schafer, D.A., and Bear, J.E. (2007). Coronin 1B
692 Coordinates Arp2/3 Complex and Cofilin Activities at the Leading Edge. Cell *128*, 915–929.

23

693   Chen, Y.-K., and Hsueh, Y.-P. (2012). Cortactin-Binding Protein 2 Modulates the Mobility of

694   Cortactin and Regulates Dendritic Spine Formation and Maintenance. J. Neurosci. *32*, 1043–

695   1055.

696   Chen, Y.-K., Chen, C.-Y., Hu, H.-T., and Hsueh, Y.-P. (2012). CTTNBP2, but not CTTNBP2NL,

697   regulates dendritic spinogenesis and synaptic distribution of the striatin–PP2A complex. Mol.

698   Biol. Cell *23*, 4383–4392.

699   Currie, J.D., and Rogers, S.L. (2011). Using the Drosophila melanogaster D17-c3 cell culture

700   system to study cell motility. Nat. Protoc. *6*, 1632–1641.

701   Danuser, G., and Waterman-Storer, C.M. (2006). Quantitative Fluorescent Speckle Microscopy

702   of Cytoskeleton Dynamics. Annu. Rev. Biophys. Biomol. Struct. *35*, 361–387.

703   Ferreira, T.A., Blackman, A.V., Oyrer, J., Jayabal, S., Chung, A.J., Watt, A.J., Sjöström, P.J.,

704   and van Meyel, D.J. (2014). Neuronal morphometry directly from bitmap images. Nat. Methods

705   *11*, 982–984.

706   Fischer, M., Kaech, S., Knutti, D., and Matus, A. (1998). Rapid Actin-Based Plasticity in

707   Dendritic Spines. Neuron *20*, 847–854.

708   Flockhart, I., Booker, M., Kiger, A., Boutros, M., Armknecht, S., Ramadan, N., Richardson, K.,

709   Xu, A., Perrimon, N., and Mathey-Prevot, B. (2006). FlyRNAi: the Drosophila RNAi screening

710   center database. Nucleic Acids Res. *34*, D489-494.

711   Gelbart, W.M., and Emmert, D.B. (2013). FlyBase High Throughput Expression Pattern Data.

712   Goley, E.D., and Welch, M.D. (2006). The ARP2/3 complex: an actin nucleator comes of age.

713   Nat. Rev. Mol. Cell Biol. *7*, 713–726.

714   Goujon, M., McWilliam, H., Li, W., Valentin, F., Squizzato, S., Paern, J., and Lopez, R. (2010). A

715   new bioinformatics analysis tools framework at EMBL–EBI. Nucleic Acids Res. *38*, W695–

716   W699.

717   Harms, B.D., Bassi, G.M., Horwitz, A.R., and Lauffenburger, D.A. (2005). Directional

718   Persistence of EGF-Induced Cell Migration Is Associated with Stabilization of Lamellipodial

719   Protrusions. Biophys. J. *88*, 1479–1488.

720   Helgeson, L.A., and Nolen, B.J. (2013). Mechanism of synergistic activation of Arp2/3 complex
721   by cortactin and N-WASP. eLife *2*, e00884.

722   Hinz, B., Alt, W., Johnen, C., Herzog, V., and Kaiser, H.W. (1999). Quantifying lamella dynamics
723   of cultured cells by SACED, a new computer-assisted motion analysis. Exp. Cell Res. *251*, 234–
724   243.

725   Hirakawa, H., Shibata, K., and Nakayama, T. (2009). Localization of cortactin is associated with
726   colorectal cancer development. Int. J. Oncol. *35*, 1271–1276.

727   Hostos, E.L. de, Rehfuess, C., Bradtke, B., Waddell, D.R., Albrecht, R., Murphy, J., and
728   Gerisch, G. (1993). Dictyostelium mutants lacking the cytoskeletal protein coronin are defective
729   in cytokinesis and cell motility. J. Cell Biol. *120*, 163–173.

730   Hotulainen, P., and Hoogenraad, C.C. (2010). Actin in dendritic spines: connecting dynamics to
731   function. J. Cell Biol. *189*, 619–629.

732   Iwasa, J.H., and Mullins, R.D. (2007). Spatial and Temporal Relationships between Actin-
733   Filament Nucleation, Capping, and Disassembly. Curr. Biol. *17*, 395–406.

734   Kirkbride, K.C., Sung, B.H., Sinha, S., and Weaver, A.M. (2011). Cortactin. Cell Adhes. Migr. *5*,
735   187–198.

736   Krause, M., and Gautreau, A. (2014). Steering cell migration: lamellipodium dynamics and the
737   regulation of directional persistence. Nat. Rev. Mol. Cell Biol. *15*, nrm3861.

738   Lai, F.P., Szczodrak, M., Block, J., Faix, J., Breitsprecher, D., Mannherz, H.G., Stradal, T.E.,
739   Dunn, G.A., Small, J.V., and Rottner, K. (2008). Arp2/3 complex interactions and actin network
740   turnover in lamellipodia. EMBO J. *27*, 982–992.

741   Longair, M.H., Baker, D.A., and Armstrong, J.D. (2011). Simple Neurite Tracer: open source
742   software for reconstruction, visualization and analysis of neuronal processes. Bioinformatics *27*,
743   2453–2454.

744   Lu, W., Castillo, U. del, and Gelfand, V.I. (2013). Organelle Transport in Cultured Drosophila
745   Cells: S2 Cell Line and Primary Neurons. JoVE J. Vis. Exp. e50838–e50838.

746 MacGrath, S.M., and Koleske, A.J. (2012). Cortactin in cell migration and cancer at a glance. J
747 Cell Sci *125*, 1621–1626.

748 Machesky, L.M., Mullins, R.D., Higgs, H.N., Kaiser, D.A., Blanchoin, L., May, R.C., Hall, M.E.,
749 and Pollard, T.D. (1999). Scar, a WASp-related protein, activates nucleation of actin filaments
750 by the Arp2/3 complex. Proc. Natl. Acad. Sci. *96*, 3739–3744.

751 Mahaffy, R.E., and Pollard, T.D. (2006). Kinetics of the Formation and Dissociation of Actin
752 Filament Branches Mediated by Arp2/3 Complex. Biophys. J. *91*, 3519–3528.

753 Martin, A.C., Welch, M.D., and Drubin, D.G. (2006). Arp2/3 ATP hydrolysis-catalysed branch
754 dissociation is critical for endocytic force generation. Nat. Cell Biol. *8*, 826–833.

755 Matus, A. (2000). Actin-Based Plasticity in Dendritic Spines. Science *290*, 754–758.

756 Mendoza, M.C., Besson, S., and Danuser, G. (2012). Quantitative Fluorescent Speckle
757 Microscopy (QFSM) to Measure Actin Dynamics. Curr. Protoc. Flow Cytom. *2.18*.

758 Mullins, R.D., Stafford, W.F., and Pollard, T.D. (1997). Structure, Subunit Topology, and Actin-
759 binding Activity of the Arp2/3 Complex from Acanthamoeba. J. Cell Biol. *136*, 331–343.

760 Ohoka, Y., and Takai, Y. (1998). Isolation and characterization of cortactin isoforms and a novel
761 cortactin-binding protein, CBP90. Genes Cells *3*, 603–612.

762 Patel, A.S., Schechter, G.L., Wasilenko, W.J., and Somers, K.D. (1998). Overexpression of
763 EMS1/cortactin in NIH3T3 fibroblasts causes increased cell motility and invasion in vitro.
764 Oncogene *16*, 3227–3232.

765 Prehoda, K.E., Scott, J.A., Dyche Mullins, R., and Lim, W.A. (2000). Integration of Multiple
766 Signals Through Cooperative Regulation of the N-WASP-Arp2/3 Complex. Science *290*, 801–
767 806.

768 Ren, G., Crampton, M.S., and Yap, A.S. (2009). Cortactin: Coordinating adhesion and the actin
769 cytoskeleton at cellular protrusions. Cell Motil. Cytoskeleton *66*, 865–873.

770 Ridley, A.J., Schwartz, M.A., Burridge, K., Firtel, R.A., Ginsberg, M.H., Borisy, G., Parsons, J.T.,
771 and Horwitz, A.R. (2003). Cell Migration: Integrating Signals from Front to Back. Science *302*,
772 1704–1709.

26

773   Rogers, S.L., and Rogers, G.C. (2008). Culture of Drosophila S2 cells and their use for RNAi-
774   mediated loss-of-function studies and immunofluorescence microscopy. Nat. Protoc. *3*, 606–
775   611.

776   Rogers, S.L., Wiedemann, U., Stuurman, N., and Vale, R.D. (2003). Molecular requirements for
777   actin-based lamella formation in Drosophila S2 cells. J. Cell Biol. *162*, 1079–1088.

778   Rothschild, B.L., Shim, A.H., Ammer, A.G., Kelley, L.C., Irby, K.B., Head, J.A., Chen, L.,
779   Varella-Garcia, M., Sacks, P.G., Frederick, B., et al. (2006). Cortactin Overexpression
780   Regulates Actin-Related Protein 2/3 Complex Activity, Motility, and Invasion in Carcinomas with
781   Chromosome 11q13 Amplification. Cancer Res. *66*, 8017–8025.

782   Shih, P.-Y., Lee, S.-P., Chen, Y.-K., and Hsueh, Y.-P. (2014). Cortactin-binding protein 2
783   increases microtubule stability and regulates dendritic arborization. J. Cell Sci. *127*, 3521–3534.

784   Sholl, D.A. (1953). Dendritic organization in the neurons of the visual and motor cortices of the
785   cat. J. Anat. *87*, 387–406.1.

786   Sievers, F., Wilm, A., Dineen, D., Gibson, T.J., Karplus, K., Li, W., Lopez, R., McWilliam, H.,
787   Remmert, M., Söding, J., et al. (2011). Fast, scalable generation of high-quality protein multiple
788   sequence alignments using Clustal Omega. Mol. Syst. Biol. *7*, 539.

789   Singh, P.P., Hawthorne, J.L., Davis, C.A., and Quintero, O.A. (2016). Permeabilization Activated
790   Reduction in Fluorescence (PARF): a novel method to measure kinetics of protein interactions
791   with intracellular structures. Cytoskelet. Hoboken NJ *73*, 271–285.

792   Siton, O., Ideses, Y., Albeck, S., Unger, T., Bershadsky, A.D., Gov, N.S., and Bernheim-
793   Groswasser, A. (2011). Cortactin Releases the Brakes in Actin- Based Motility by Enhancing
794   WASP-VCA Detachment from Arp2/3 Branches. Curr. Biol. *21*, 2092–2097.

795   Suraneni, P., Rubinstein, B., Unruh, J.R., Durnin, M., Hanein, D., and Li, R. (2012). The Arp2/3
796   complex is required for lamellipodia extension and directional fibroblast cell migration. J Cell Biol
797   *197*, 239–251.

798   Svitkina, T. (2016). Imaging Cytoskeleton Components by Electron Microscopy. Methods Mol.
799   Biol. *1365,* 99-118.

800   Svitkina, T.M., and Borisy, G.G. (1999). Arp2/3 Complex and Actin Depolymerizing

801   Factor/Cofilin in Dendritic Organization and Treadmilling of Actin Filament Array in Lamellipodia.

802   J. Cell Biol. *145*, 1009–1026.

803   Svitkina, T.M., Bulanova, E.A., Chaga, O.Y., Vignjevic, D.M., Kojima, S., Vasiliev, J.M., and

804   Borisy, G.G. (2003). Mechanism of filopodia initiation by reorganization of a dendritic network. J

805   Cell Biol *160*, 409–421.

806   Uruno, T., Liu, J., Zhang, P., Fan, Y., Egile, C., Li, R., Mueller, S.C., and Zhan, X. (2001).

807   Activation of Arp2/3 complex-mediated actin polymerization by cortactin. Nat. Cell Biol. *3*, 259–

808   266.

809   Uruno, T., Liu, J., Li, Y., Smith, N., and Zhan, X. (2003). Sequential Interaction of Actin-related

810   Proteins 2 and 3 (Arp2/3) Complex with Neural Wiscott-Aldrich Syndrome Protein (N-WASP)

811   and Cortactin during Branched Actin Filament Network Formation. J. Biol. Chem. *278*, 26086–

812   26093.

813   Weaver, A.M. (2008). Cortactin in tumor invasiveness. Cancer Lett. *265*, 157–166.

814   Weaver, A.M., Karginov, A.V., Kinley, A.W., Weed, S.A., Li, Y., Parsons, J.T., and Cooper, J.A.

815   (2001). Cortactin promotes and stabilizes Arp2/3-induced actin filament network formation. Curr.

816   Biol. CB *11*, 370–374.

817   Weaver, A.M., Heuser, J.E., Karginov, A.V., Lee, W., Parsons, J.T., and Cooper, J.A. (2002).

818   Interaction of Cortactin and N-WASp with Arp2/3 Complex. Curr. Biol. *12*, 1270–1278.

819   Wu, C., Asokan, S.B., Berginski, M.E., Haynes, E.M., Sharpless, N.E., Griffith, J.D., Gomez,

820   S.M., and Bear, J.E. (2012). Arp2/3 Is Critical for Lamellipodia and Response to Extracellular

821   Matrix Cues but Is Dispensable for Chemotaxis. Cell *148*, 973–987.

822   Xu, X.-Z., Garcia, M.V., Li, T., Khor, L.-Y., Gajapathy, R.S., Spittle, C., Weed, S., Lessin, S.R.,

823   and Wu, H. (2010). Cytoskeleton alterations in melanoma: aberrant expression of cortactin, an

824   actin-binding adapter protein, correlates with melanocytic tumor progression. Mod. Pathol. Off.

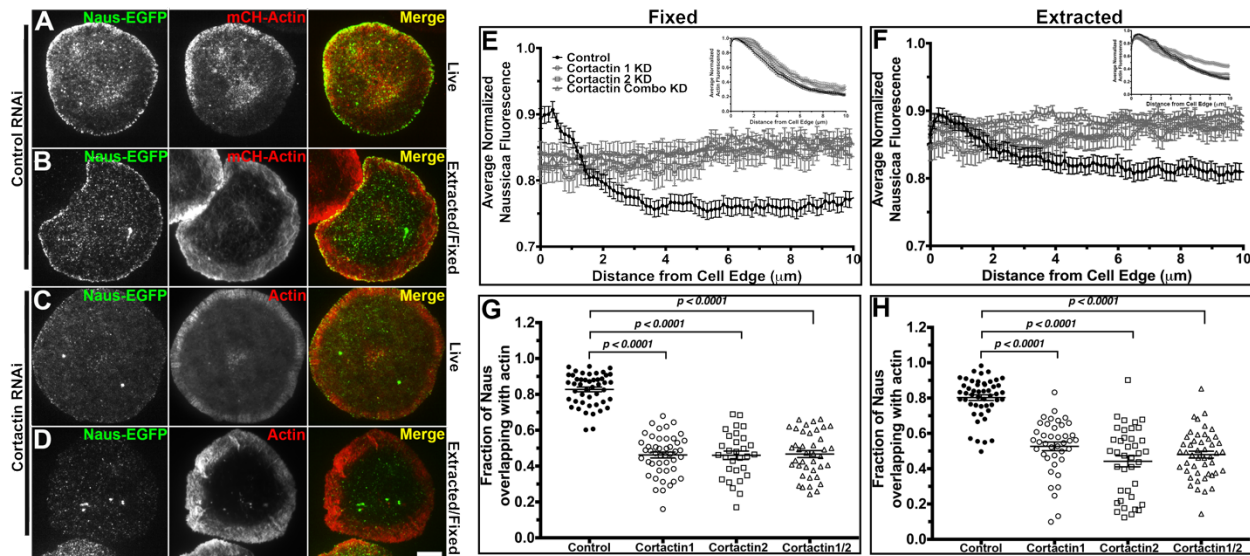825   J. U. S. Can. Acad. Pathol. Inc *23*, 187–196.

826   Zalevsky, J., Lempert, L., Kranitz, H., and Mullins, R.D. (2001). Different WASP family proteins

827   stimulate different Arp2/3 complex-dependent actin-nucleating activities. Curr. Biol. *11*, 1903–

828   1913.

829

830

831   **Figures.**

832

833

834   **Figure 1. Nausicaa's lamellipodial localization is Cortactin-dependent.** (A & B) Control RNAi treated S2R+ cells

835   transfected with Naus-EGFP (left panels, green in merged image) and mCherry-Actin (middle panels, red in the

836   merged image) imaged live (A) or extracted with detergent prior to fixation and stained with phalloidin (middle panels,

837   red in the merged image) to visualize F-actin (B). (C & D) Cortactin RNAi treated S2R+ cells transfected with Naus-

838   EGFP (left panels, green in the merged images) and mCherry-Actin (middle panels, red in the merged image) imaged

839   live (C) or extracted with detergent prior to fixation and stained with phalloidin (middle panels, red in the merged

840   images) to visualize F-actin (D). Scale bar = 10 µm. (E) Line scan analysis of the lamellipodial distribution of Naus-

841   EGFP in fixed S2R+ cells treated with control RNAi (black circles), or Cortactin RNAi from two independent RNAi

842   targets (open gray circles or squares) or the combination of the two targets (open gray triangles). Inset is the

843   corresponding averaged normalized actin fluorescence. Error bars denote S.E.M. (F) Line scan analysis of the

844   lamellipodial distribution of Naus-EGFP in cells that were extracted with detergent prior to fixation following control

845   RNAi (black circles) or treatment with two independent Cortactin RNAi targets (open gray circles or squares) or the

846   combination of the two (open gray triangles). Inset is the corresponding averaged normalized actin fluorescence.

847   Error bars denote S.E.M. (G) Mander's coefficient of the amount of overlap between Naus-EGFP and F-actin stained

848   by phalloidin. Cells were treated with control RNAi (black circles) or one of two Cortactin RNAi targets (open gray

849   circles or squares) or the combination of the two (open gray triangles). There was a statistically significant decrease

850   in lamellipodial enrichment when cells were depleted of Cortactin (error bars = S.E.M., n = 30-45 cells per condition)

851   (*** = p-value <0.0001, Student's t-test). (H) Mander's coefficient quantifying the amount of overlap between Naus-

852   EGFP and F-actin as visualized by phalloidin in cells that were first extracted prior to fixation. control RNAi is shown

853   in black circles, Cortactin RNAi (from two independent targets) is shown in open gray circles or squares, and the

854   combination of the two Cortactin RNAi targets is shown in open gray triangles. There was a statistically significant

855   decrease in the amount of overlap between Naus-EGFP and F-actin stained by phalloidin (error bars are S.E.M, n=

856   40-50 cells per condition) (*** = p-value < 0.0001, Student's t-test).
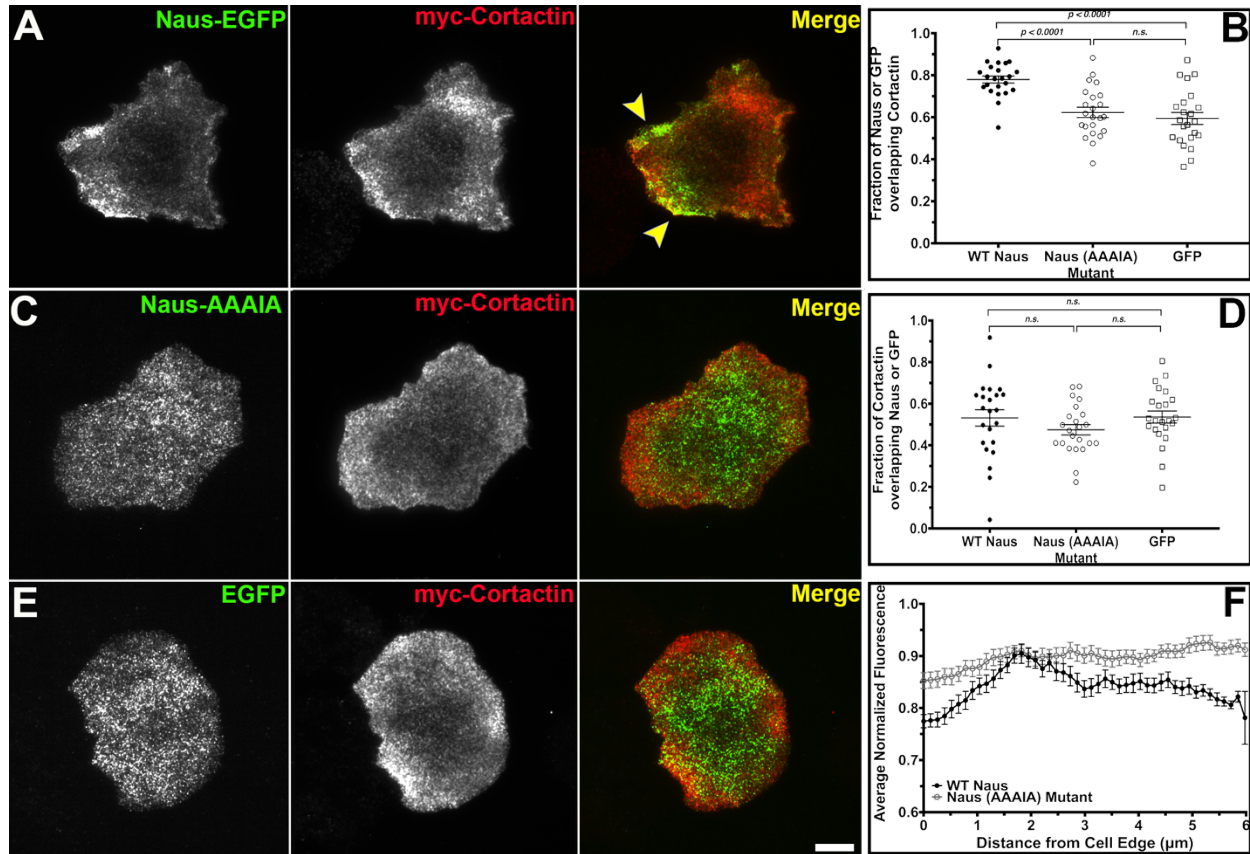
857

858

859

860
861
862

863
864

865 **Figure 2. Nausicaa colocalizes with Cortactin through a conserved proline rich motif.** (A-C) Fixed S2R+ cells
866 co-transfected with myc-Cortactin and either Naus-EGFP (A), Naus(AAAIA)-EGFP mutant (B), or EGFP control (C)
867 (left panels, green in merged images) and stained with anti-Myc (middle panels, red in merged images). Yellow
868 arrowheads in A indicate regions of colocalization between Naus-EGFP and myc-Cortactin. Scale bar = 10 μm. (D)
869 Mander's coefficient analysis for Naus or EGFP constructs overlapping with Myc-Cortactin (*** = p-value < 0.0001,
870 One-way ANOVA, error bars = S.E.M., n=23 cells per condition). (E) Mander's coefficient analysis for Cortactin
871 overlapping with Naus or EGFP constructs. None of these differences were statistically significant (n.s.). (F) Line
872 scan analysis of the lamellipodial distribution of WT Naus-EGFP (black circles) or Naus-EGFP AAAIA (open gray
873 circles) in fixed S2R+ cells (error bars denote S.E.M., n= 23 cells per condition).

874
875

31
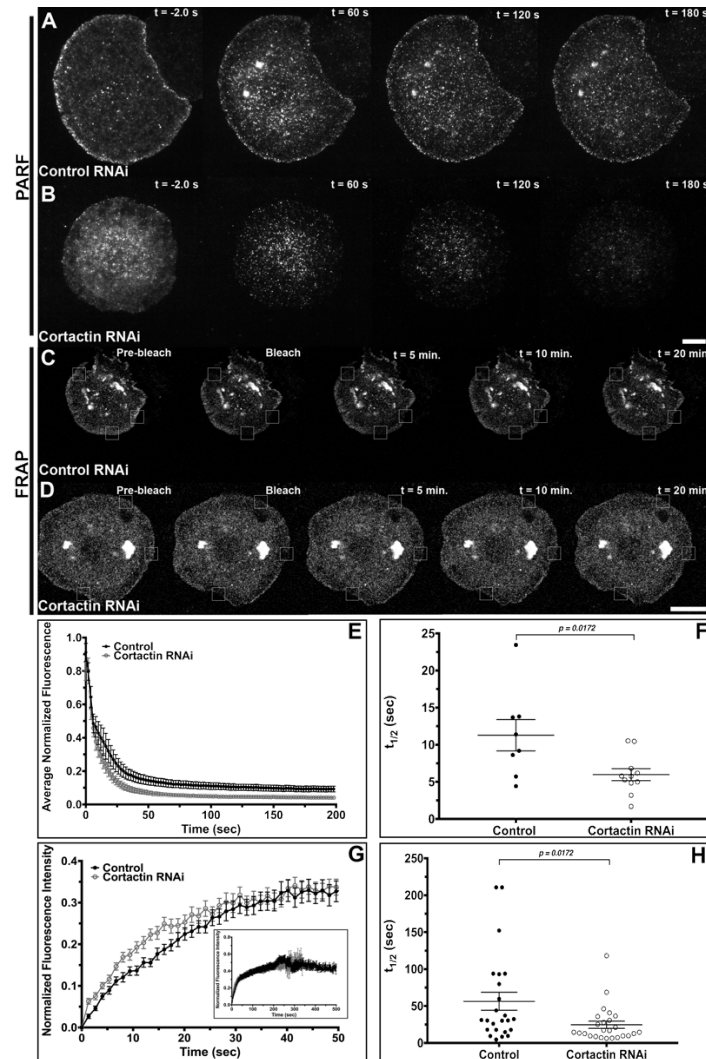
Figure 3. Depletion of Cortactin alters Nausicaa dynamics in the lamellipodia of S2R+ cells. (A-B) Time-lapse images of permeabilization activated reduction in fluorescence (PARF) in S2R+ cells transfected with Naus-EGFP following Control RNAi (A) or Cortactin RNAi (B) treatments. (C-D) Time-lapse images of fluorescence recovery after photobleaching (FRAP) of S2R+ cells transfected with Naus-EGFP following (C) Control RNAi or (D) Cortactin RNAi treatments. Small white boxes denote regions bleached. Scale bar = 10 μm (E) Average normalized fluorescence decay from PARF experiments. Error bars denote S.E.M. (F) Average half-life of Naus-EGFP fluorescence for Control (black circles) or Cortactin RNAi (open gray circles) conditions from PARF experiments. The fluorescent decay from Cortactin depleted cells was statistically significantly faster than control RNAi treated cells (p-value = 0.0172, Student's t-test, Control: n = 8 cells, Cortactin RNAi: n = 11 cells). (G) Average normalized fluorescence recovery from FRAP experiments, in black circles, control RNAi and open gray circles, Cortactin RNAi. (H) Average half-life of Naus-EGFP fluorescence recovery for control (black circles) or Cortactin RNAi (open gray circles) treated cells from the FRAP experiments. Cortactin depleted cells recovered statistically significantly faster than control cells (p-value = 0.0178, Student's t-test, Control: n = 24 cells, Cortactin RNAi: n = 25 cells). Error bars are S.E.M.

32
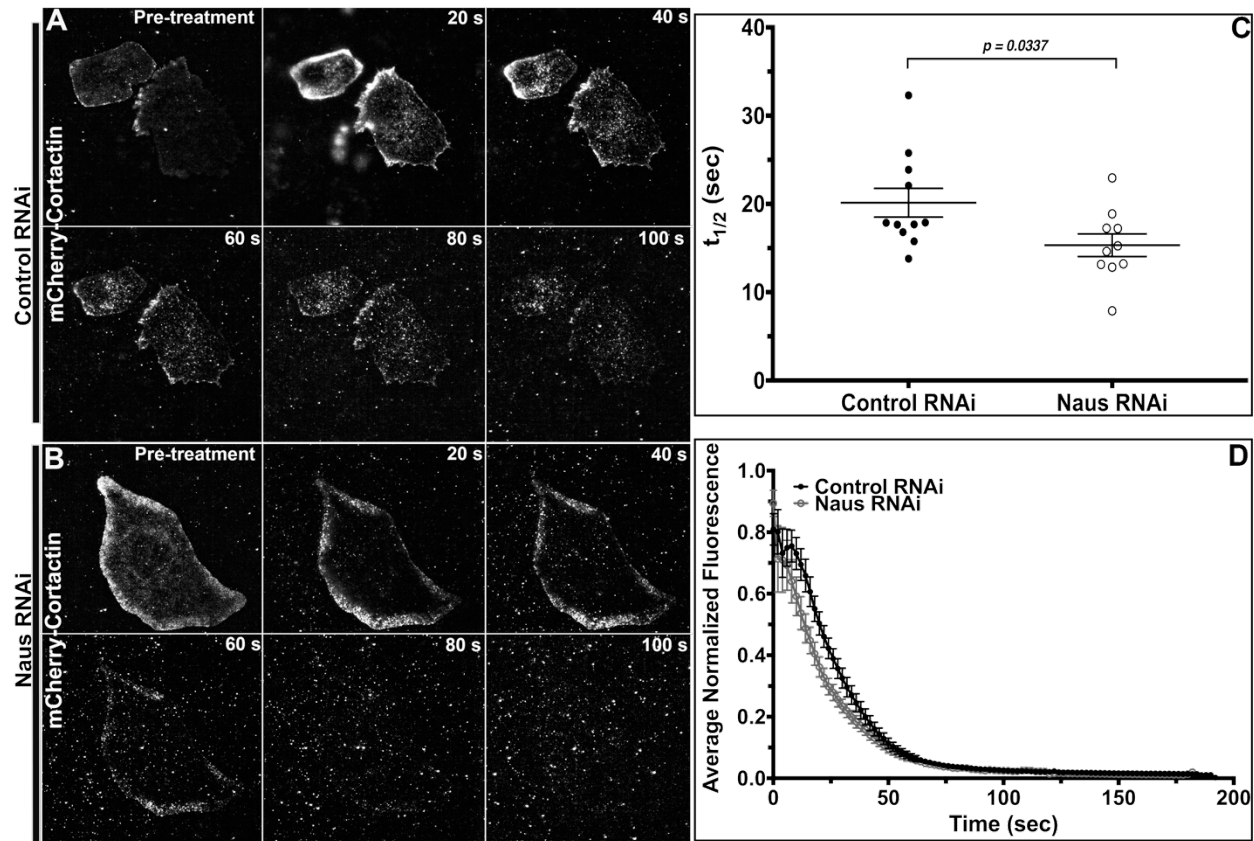
Figure 4. Depletion of Nausicaa alters Cortactin dynamics in S2R+ cells. (A & B) Time-lapse images of permeabilization activated reduction in fluorescence (PARF) of S2R+ cells transfected with mCherry-Cortactin following control RNAi (A) or Naus RNAi (B) treatments. (C) Average half-life of mCherry-Cortactin fluorescence for control (black circles) or Naus RNAi (open gray circles) treatments. Cortactin's fluorescence decay was a statistically significantly faster following Naus RNAi as compared to control RNAi treated cells (*p-value 0.0337, Student's t-test, Control: n = 10 cells, Naus RNAi: n = 11 cells). (D) Average normalized mCherry-Cortactin fluorescence decay from PARF experiments. Error bars denote S.E.M.. Scale bar = 10 µm.
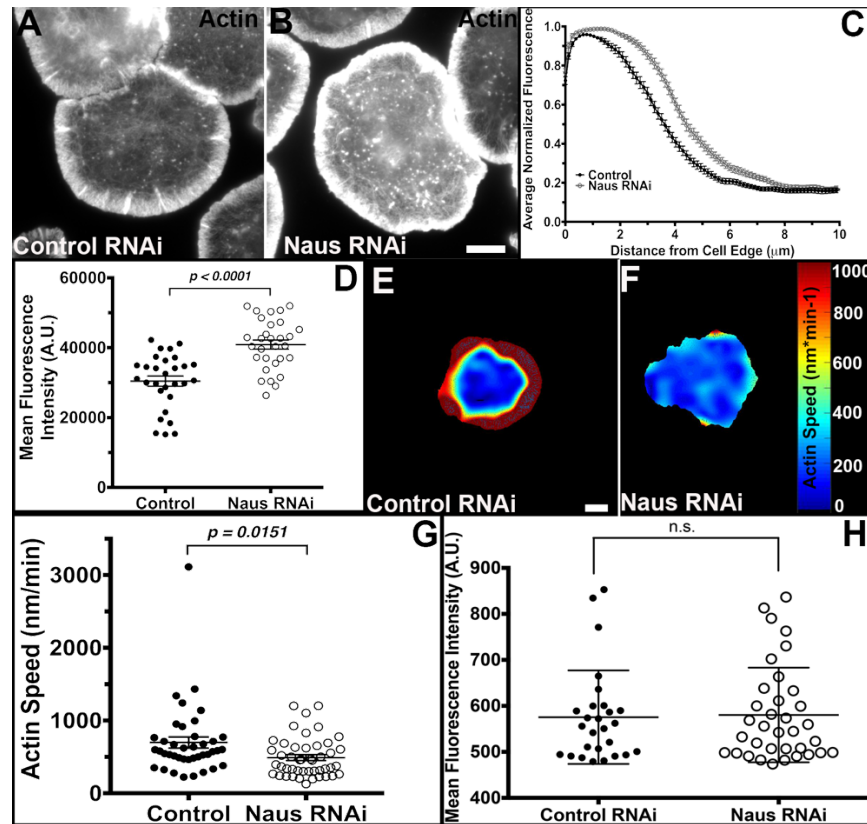
33

Figure 5. Nausicaa regulates lamellipodial actin density and actin retrograde flow in S2R+ cells. (A & B) Fixed S2R+ cells treated with control (A) or Naus (B) RNAi stained for F-actin with phalloidin. Gray levels have been set equal for comparison. Scale bars = 10 μm. (C) Line scan analysis of F-actin fluorescence in the lamellipodia from cells as shown in A & B. Fluorescence was normalized for each cell and averaged for each condition (black circles control RNAi and open gray circles Naus RNAi). (D) Mean fluorescence intensity of lamellipodial actin of cells treated with control RNAi (black circles) or Naus RNAi (open gray circles) from cells as shown in A & B. Naus RNAi led to a statistically significant increase in the F-actin fluorescence throughout the lamellipodial (**p-value <0.0001, Student's t-test, n = 30 cells per condition). (E & F) Representative heat maps of actin speeds in control (E) or Naus (F) RNAi treated cells from QFSM analysis. Cool colors indicate slower rates of retrograde flow and warm colors represent faster speeds of actin retrograde flow. Scale bar = 10 μm. (G) Quantification of lamellipodial actin speeds from QFSM analysis. Naus depletion led to a statistically significant decrease in the rate of actin retrograde flow rates (*p-value 0.0151, Student's t-test, Control RNAi: n = 40 cells, Naus RNAi: n = 46 cells). (H) Quantification of the mean fluorescence intensity of EGFP-Actin in the cells analyzed by QFSM (black circles control RNAi and open gray circles Naus RNAi). There was not a statistically significant difference between control and Naus RNAi treated cells.
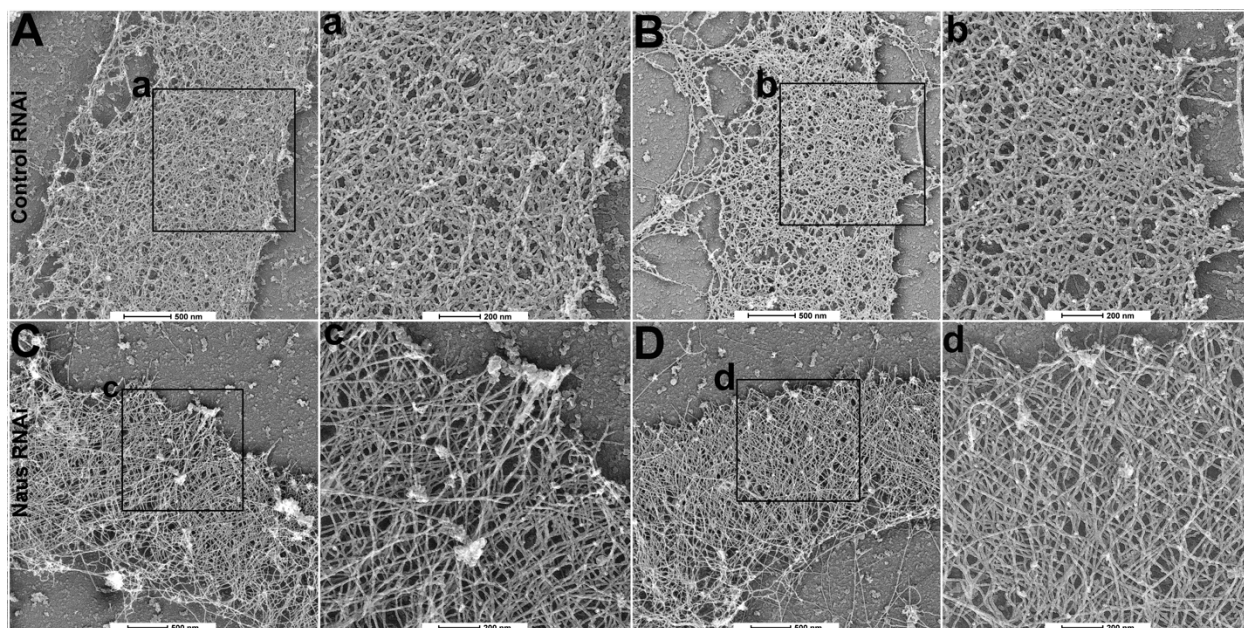
Figure 6. Depletion of Naus leads to an increase in the number of long, unbranched actin filaments on the lamellipodia. Platinum replicas of the lamellipodia of S2R+ cells treated with control (A & B) or Naus (C & D) RNAi. The black box denotes the region shown at higher magnification (control RNAi shown in a & b and Naus RNAi shown in c & d). Scale bars are given for each image. Scale bar in lower magnification images (A, B, C, D) 500 nm, scale bar in higher magnification images (a, b, c, d) 200 nm.

35

923
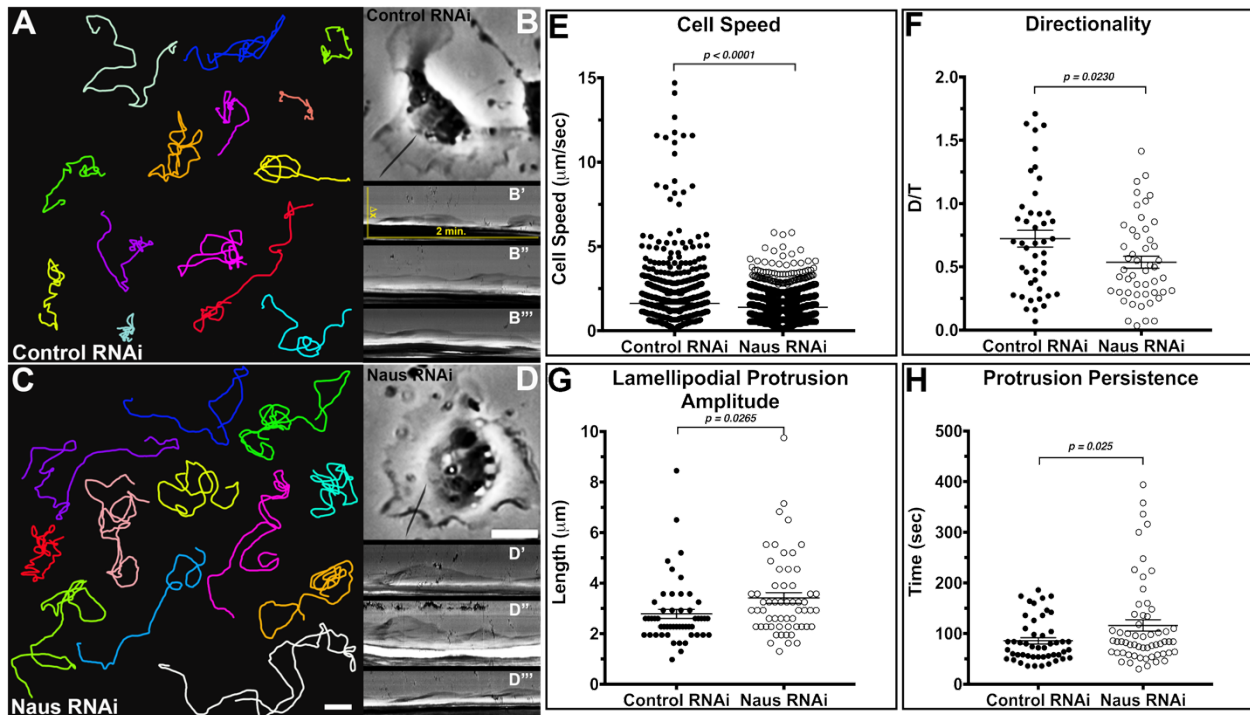
924
925 **Figure 7. Nausicaa regulates directionality and lamellipodial persistence in migrating D25c2 cells.** (A-D)
926 Representative migration tracks for *Drosophila* D25 cells treated with control (A & B) or Naus (C & D) RNAi. (B'-B''')
927 Representative kymographs from control RNAi treated D25 cells, the black line represents a typical region of
928 interested used to generate kymographs. (D'-D''') Representative kymographs for Naus RNAi treated D25 cells, the
929 black line represents a typical region of interested used to generate kymographs. (E) Average instantaneous cell
930 speeds for control or Naus RNAi treated D25 cells. Naus depletion led to a slight, but statistically significant reduction
931 in cell migration speeds (***p-value <0.0001, Student's t-test, Control: n = 43 cells, 1438 measurements, Naus RNAi:
932 n = 50 cells, 1779 measurements). (F) Directionality, was measured as the ratio of D/T where D is distance between
933 starting and end point and T is the total distance traveled. Naus depleted cells showed a statistically significant
934 reduction in directionality as compared to control RNAi treated cells (*p-value = 0.0230, Student's t-test, Control: n =
935 44 cells, Naus RNAi: n = 49 cells). (G) Naus RNAi led to an increase in the length of lamellipodial protrusions as
936 compared to control RNAi treated D25 cells (*p-value = 0.0265, Student's t-test, Control: n = 51 cells, Naus RNAi: n =
937 58 cells). (H) Protrusion persistence was increased upon treatment with Naus RNAi as compared to control treated
938 D25 cells (*p-value = 0.025, Student's t-test, Control RNAi: n = 49 cells, Naus RNAi: n = 59 cells). All error bars =
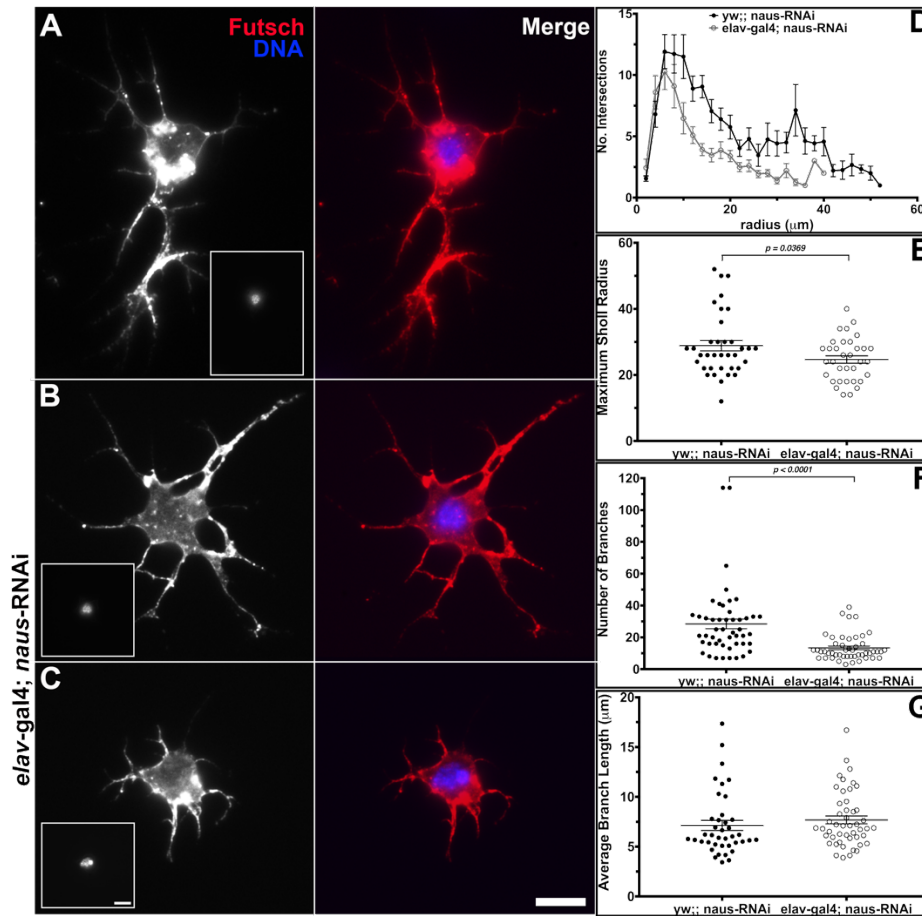939 S.E.M. Scale bar = 10 µm.

940
941
942
943
944
945
946
947

36

948

949
950 **Figure 8. Nausicaa regulates neuronal morphology in 3rd instar larvae neurons.** (A-C) Primary neuroblasts from
951 3rd instar larvae were harvested and allowed to differentiate for 24 hours in culture. They were then fixed and
952 stained for microtubules (anti-Futsch, red in merged images) and DNA (Hoechst, inset and in blue in merged
953 images). (A) Control neurons from yw;; *naus*-RNAi flies. (B & C) Neurons from flies expressing *naus*-RNAi driven by
954 *elav*-gal4. Scale bars = 10 µm.(D) Naus depletion also led to a decrease in the Sholl profile, which measures the
955 number of intersections a neuron makes, (error bars denote S.E.M.). (E) The maximum Sholl radius, which measures
956 the number of branch intersections from concentric circles also indicated a decrease in Naus RNAi neurons (open
957 gray circles) as compared to control neurons (black circles) (*p-value = 0.0369, Student's t-test, control: n = 36 cells,
958 Naus RNAi: n = 34 cells). (F & G) 2D skeletons of neurons were manually drawn and analyzed ImageJ Simple
959 Neurite Tracer for (F) number of branches and (G) the average branch length. (F) There was a statistically significant
960 decrease in the average number of branches in Naus depleted neurons (open gray circles) as compared to control
961 neurons (black circles) prepared in parallel (***p-value <0.0001, Student's t-test, Control: n = 49 cells, Naus RNAi: n =
962 48 cells). (G) The average branch length was not significantly different between control (black circles) and Naus RNAi
963 (open gray circles) neurons . Error bars = S.E.M.

964
965
966
967
968
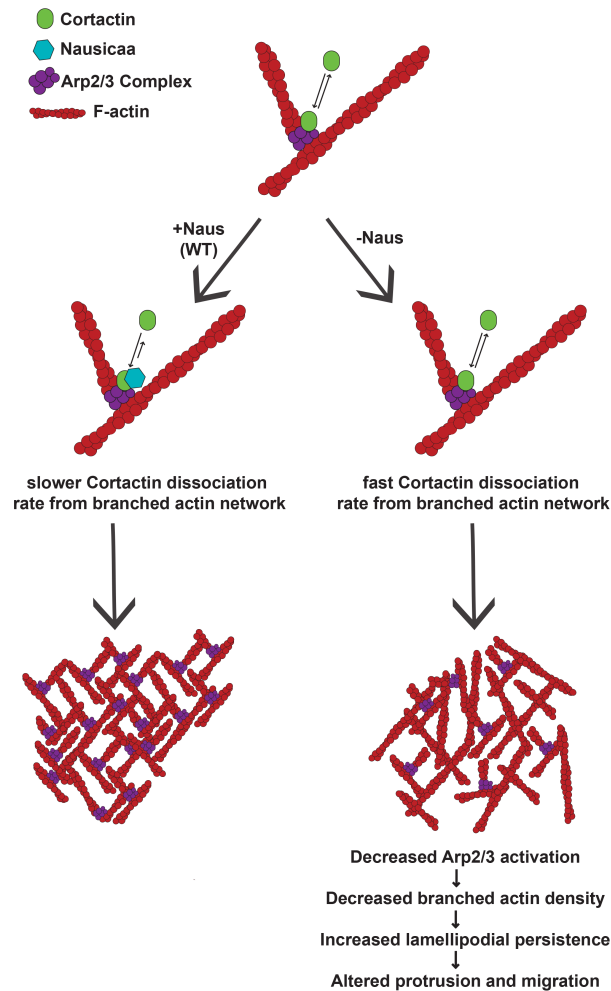
Figure 9. Proposed model of Nausicaa's role in the lamellipodia. Nausicaa works to stabilize Cortactin at Arp2/3 generated branches in order to appropriately regulate branch density of the lamellipodia. Nausicaa's interaction with Cortactin maintains Cortactin on branched actin networks and stabilizes these junctions. In the absence of Nausicaa, Cortactin has a fast off-rate from Arp2/3 branches (Helgeson and Nolen, 2013). Cortactin more freely diffuses leading to a decrease in the activation of the Arp2/3 complex and a loss of branch stability. This increased filament length eads to larger lamellipodial protrusions and downstream alterations to migration and morphology.

984

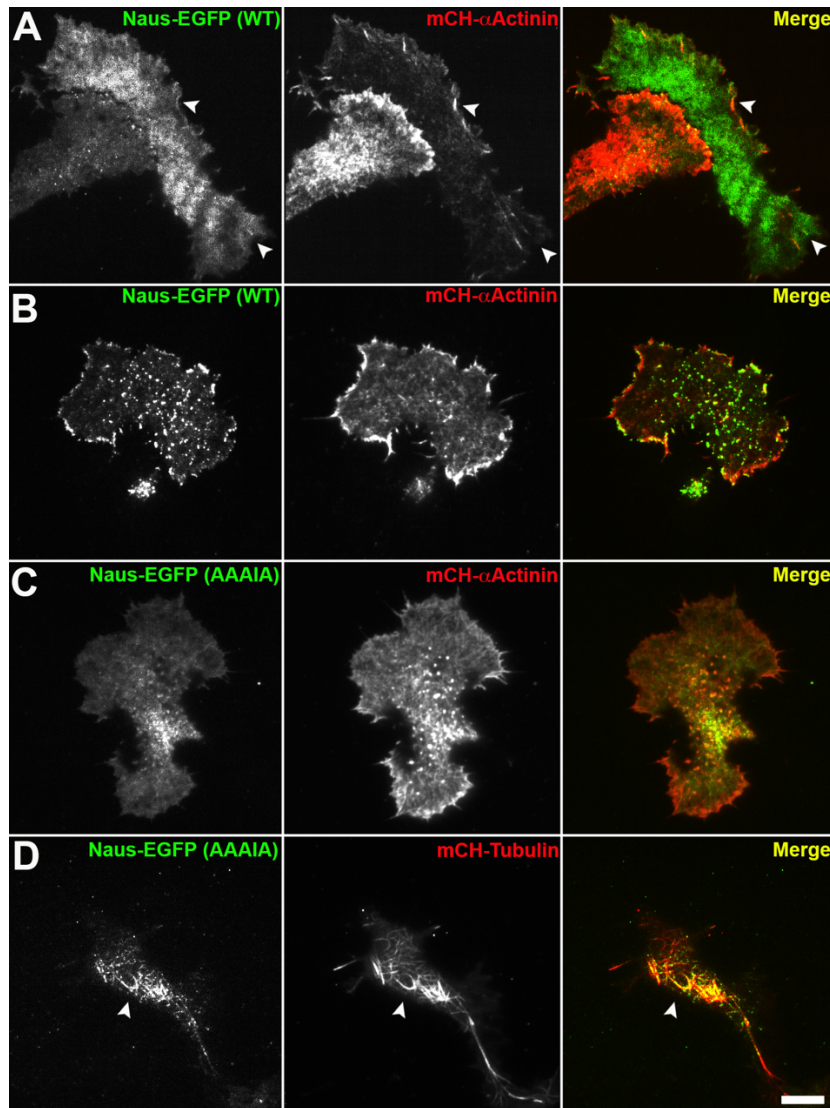985 **Supplemental Figures and Tables.**

986

987 **Supplemental Table 1.** Forward and reverse primer sequences for production of cloning and
988 dsDNA (for dsRNA production) used in this study.

| Gene Name	CG Number	Use	Forward Primer (5'-3')	Reverse Primer (5'-3')	Reference
p20 of Arp2/3 complex	CG5972	dsDNA for RNAi	CAGACAACAACCCGACACC	CAGTTTCATTTCGCTGATCTCC	(Rogers et al., 2003)
Cortactin	CG3637	dsDNA for RNAi	ATCAGAACGCAGGATACGGA	GAGACTCGTGCTTCTCCACC	Harvard Fly RNAi (Flockhart et al., 2006)
Cortactin	CG3637	dsDNA for RNAi	AAGTCGGCTGTGGGTCATGA	CTGGCTTGACCTTGTGGTCC	This study
Cortactin	CG3637	pMT-mCherry-Cortactin	ATGTGGAAGGCAAGTGCCGGTATGTGGAAGGCAAGTGCCGGT	TTATGAGTTCTGTCCCACCACCTGC	This study
Cortactin	CG3637	pMT-myc-Cortactin	ATGGAGCAAAAACTCATTAGCGAAGAAGACTTAATGTGGAAGGCAAGTGCCGGT	TTATGAGTTCTGTCCCACCACCTGC	This study
Nausicaa	CG10915	dsDNA for RNAi	CACGAGTTCCAGACCATGAA	CCCTCTGCTTGCTAACCATC	Harvard Fly RNAi (Flockhart et al., 2006)
Nausicaa	CG10915	pIZ-Naus-EGFP	CACCATGGAGCAGAACTCGAACAGCAGCGTT	ATTCTGCTTCGCCGTGCCCGC	This study

989
990
991

Supplemental Figure 1. Sequence Alignment of *Drosophila* Nausicaa with *Homo sapien* Cortactin binding protein 2 (CTTNBP2) and Cortactin binding protein 2 N-terminal like (CTTNBP2NL). (Top) A multiple sequence alignment made using Clustal Omega comparing *Drosophila melanogaster (Dm)* Nausicaa (CG10915) and *Homo sapien (Hs)* CTTNBP2NL, and CTTNBP2. Nausicaa shares approximately 30% identity with *Hs* CTTNBP2NL and 28% identity with *Hs* CTTNBP2. Shown in red is the conserved Cortactin Binding Protein-2 (CortBP2) domain, in red italics a predicted a coiled-coil domain, and in blue the poly-proline Cortactin binding motif. Asterisks indicate identical amino acids while colons indicate similar amino acids. Note that only the first 643 amino acids of *H.s.* CTTNBP2 are shown. (Bottom) Diagram of *Dm* Nausicaa, *Hs* CTTNBP2NL and *Hs* CTTNBP2 drawn to scale. In red is the conserved CortBP2 domain, in blue the Cortactin binding motif, and in green the COOH-terminus of CTTNBP2. Note that only the first 926 amino acids of CTTNBP2 are shown.

1003
1004
1005 **Supplemental Figure 2. Nausicaa weakly localizes to α-Actinin bundles in D25c2 cells through a proline rich**
1006 **motif, while mutant Naus localizes to microtubules.** (A-D) Representative live-cell images of D25 cells co-
1007 transfected with mCherry-αActinin (A-C), or mCherry-Tubulin (D) (middle panels, red in merged images) and Naus-
1008 EGFP WT (A & B) or Naus AAAIA mutant (C & D) (left panels, green in merged images). (B) White arrowheads
1009 indicate bundled-actin structures containing both mCherry-α-Actinin and Naus-EGFP. (C) Note the loss of
1010 lamellipodial enrichment in cells expressing Naus-EGFP (AAAIA). (D) White arrowheads indicate where Naus-EGFP
1011 (AAAIA) appears to localize to microtubules. Scale bar = 10 μm.
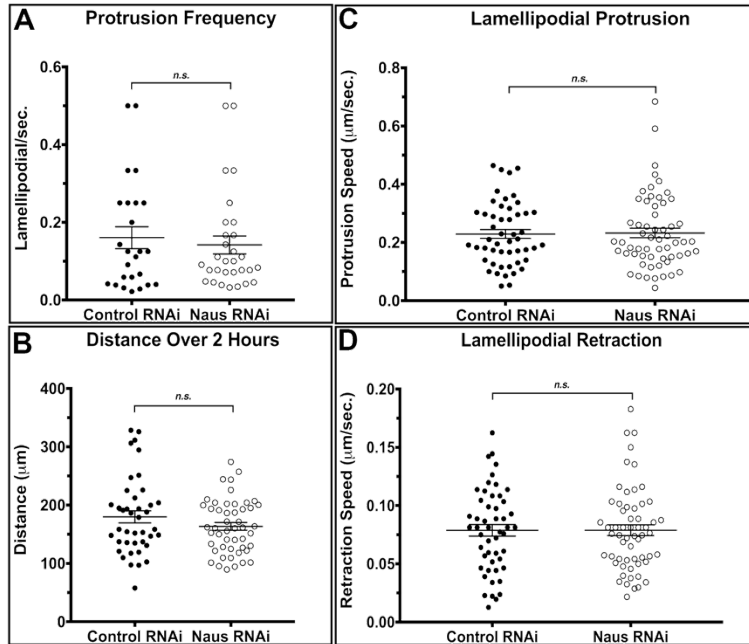
1012
1013

1014
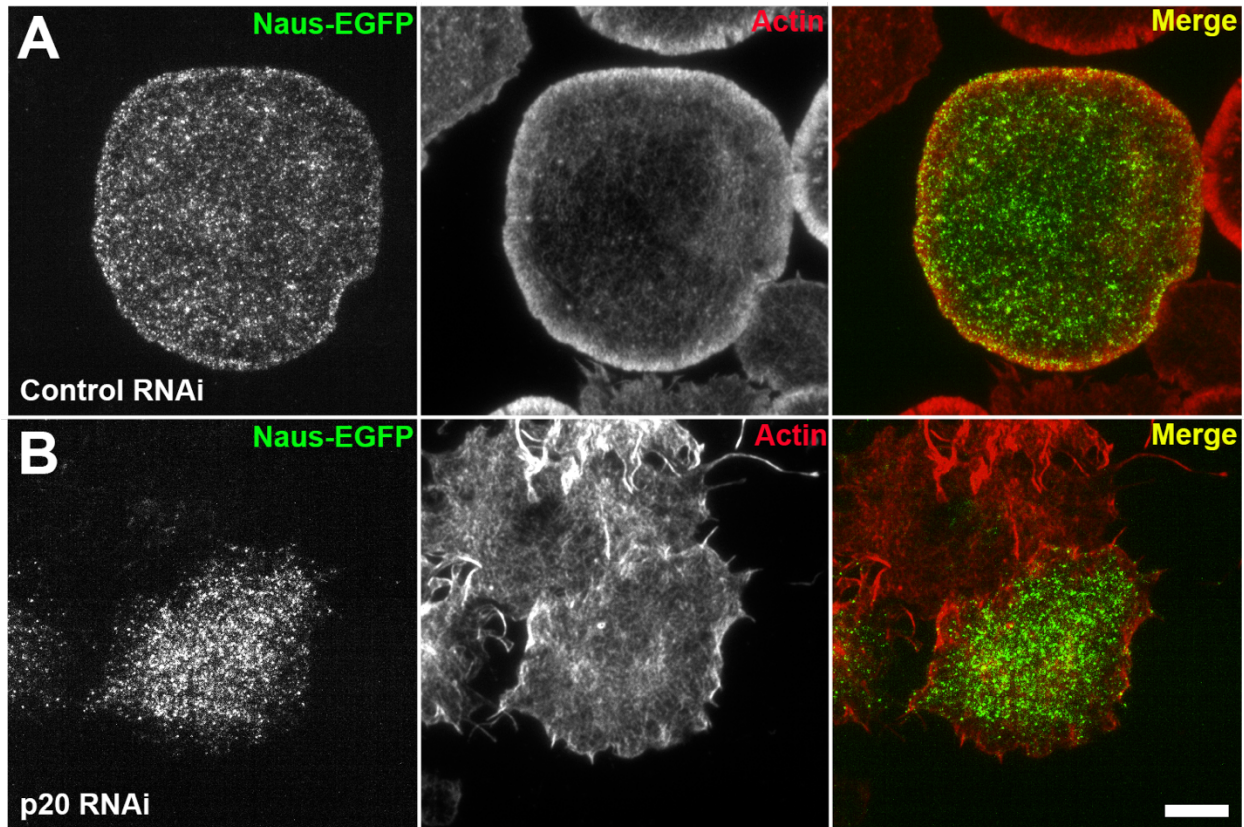
Supplemental Figure 3. Nausicaa's lamellipodial localization is dependent on Arp2/3 complex. Fixed S2R+ cells expressing Naus-EGFP (left panels, green in merged images) and treated with either control (A) or p20 (B) RNAi. Cells are stained for F-actin with phalloidin (middle panel, red in merged images). Scale bar = 10 μm.

Supplemental Figure 4. Nausicaa regulates specific lamellipodial parameters.

The parameters of lamellipodial dynamics such as frequency of protrusions (A), the distance the cells traveled over two hours (B) the speed of protrusions (C), and the speed of retractions (D) were not statistically significantly different between control and Naus treated D25 cells. N= 51 control cells and 59 Naus RNAi treated cells (A,C, and D) or N= 44 control cells and 50 Naus RNAi treated cells (B).

1028 **Supplemental Videos.**

1029 All time-lapsed images are played at a rate of 7 frames per second. All images were acquired by

1030 TIFR microscopy unless otherwise noted.

1031

1032 **Video 1. Lamellipodial localization of Naus is Cortactin-dependent.**

1033 S2R+ cells expressing EGFP-tagged Naus following control RNAi (right) or Cortactin RNAi (left).

1034 Image sequence was acquired at 3 second intervals.

1035

1036 **Video 2. PARF of Naus following treatment with control RNAi.** An S2R+ cell expressing

1037 EGFP-tagged Naus following control RNAi. After 40 seconds of imaging, the cell was

1038 permeabilized with 25 µM digitonin. Image sequence was acquired at 2 second intervals.

1039

1040 **Video 3. PARF of Naus following treatment with Cortactin RNAi.** An S2R+ cell expressing

1041 EGFP-tagged Naus following Cortactin RNAi. After 40 seconds of imaging the cell was

1042 permeabilized with 25 µM digitonin. Image sequence was acquired at 2 second intervals.

1043

1044 **Video 4. FRAP of Naus following treatment with control RNAi.** An S2R+ cell expressing

1045 EGFP-tagged Naus following control RNAi. The cell was photobleached in the regions denoted

1046 by the white boxes. The cell was imaged by an LSM 880 confocal microscope at 2 second

1047 intervals.

1048

1049 **Video 5. FRAP of Naus following treatment with Cortactin RNAi.** An S2R+ cell expressing

1050 EGFP-tagged Naus following Cortactin RNAi. The cell was photobleached in the regions

1051 denoted by the white boxes. The cell was imaged by an LSM 880 confocal microscope at 2

1052 second intervals.

1053

1054 **Video 6. PARF of Cortactin following treatment with control RNAi.** An S2R+ cell expressing

1055 mCherry-Cortactin following treatment with control RNAi. After 40 seconds of imaging the cell

1056 was permeabilized with 25 µM digitonin. Image sequence was acquired at 2 second intervals.

1057

1058 **Video 7. PARF of Cortactin following treatment with Naus RNAi.** An S2R+ cell expressing

1059 mCherry-Cortactin following treatment with Naus RNAi. After 40 seconds of imaging the cell

1060 was permeabilized with 25 µM digitonin. Image sequence was acquired at 2 second intervals.

1061

1062 **Video 8. QFSM of EGFP-actin.** Using a metallothionein promoter we titrated the addition of

1063 copper sulfate in order to generate actin speckles in S2R+ cells. When then imaged at 2 second

1064 the resulting actin dynamics following control (left) and Naus RNAi (right). Image analysis was

1065 carried out in Matlab.

1066

1067 **Video 9. Random cell motility assay.** D25 cells were treated with control or Naus RNAi for

1068 seven days and then were imaged by phase-contrast microscopy over a period of six hours.

1069 Image sequence was acquired at 5 minute intervals.